Supporting Information

Hole-Transporting Materials with a Two-Dimensionally Expanded π-System Around an Azulene Core for Efficient Perovskite Solar Cells

Hidetaka Nishimura,[†] Naoki Ishida,[‡] Ai Shimazaki,[†] Atsushi Wakamiya,[*,†,§] Akinori Saeki,[*,‡] Lawrence T. Scott,[*,||] and Yasujiro Murata[*,†]

[†]*Institute for Chemical Research, Kyoto University, Uji, Kyoto 611-0011, Japan*
[‡]*Department of Applied Chemistry, Graduate School of Engineering, Osaka University, 2-1 Yamadaoka, Suita, Osaka 565-0871, Japan*
[§]*Precursory Research for Embryonic Science and Technology (PRESTO), Japan Science and Technology Agency, 4-1-8 Honcho, Kawaguchi, Saitama 332-0012, Japan*
[||]*Merkert Chemistry Center, Boston College, Chestnut Hill, Massachusetts 02467-3860, United States*

Table of Contents

General.

Thin layer chromatography (TLC) was performed on plates coated with 0.25 mm thick silica gel 60F-254 (Merck). Column chromatography was performed using PSQ 60B (Fuji Silysia). Preparative gel permeation chromatography (GPC) was performed with a JAI LC-918 system equipped with RI-50 detector, JAIGEL-2H column (20 mm ID × 600 mm) and 1H column (20 mm ID × 600 mm) using toluene as eluent (flow rate: 3.8 mL/min). Melting points (mp) were measured on a Yanaco Micro Melting Point Apparatus. ^{1}H and ^{13}C NMR spectra were recorded with a JEOL ECA 500 (500 MHz for ^{1}H and 125 MHz for ^{13}C) spectrometers. The NMR chemical shifts are reported in ppm with reference to residual protons and carbons of $CDCl_3$ (δ 7.26 ppm in ^{1}H NMR, δ 77.0 ppm in ^{13}C NMR) and CD_2Cl_2 (δ 5.32 ppm in ^{1}H NMR, δ 53.8 ppm in ^{13}C NMR). UV-vis absorption measurement was performed with a Shimadzu UV-3150 spectrometer (Shimadzu Co.,), in degassed spectral grade solvents. Cyclic voltammetry (CV) was performed on an ALS/chi-620C electrochemical analyzer with the CV cell consisting of a glassy carbon electrode, a Pt wire counter electrode, and an $Ag/AgNO_3$ reference electrode. The measurement was carried out under an argon atmosphere using CH_2Cl_2 solutions of samples (0.5 mM) with 0.1 M tetrabutylammonium hexafluorophosphate ($Bu_4N^+PF_6^-$) as a supporting electrolyte. The redox potentials were calibrated with ferrocene as an internal standard. The HOMO energy levels in the solid state were determined from the onset of photoelectron spectra measured with a photoelectron spectrometer in air, model AC-3 (Riken Keiki Co., Ltd.). Thermogravimetric analysis (TGA) was performed on a Shimadzu TGA-50 apparatus (Shimadzu Co.,). The values are given for a weight-loss of 5% (T_{d5}). All reactions were carried out under an argon atmosphere. Photocurrent-voltage measurements (*J–V* curves) for perovskite solar cells were measured in air with an OTENTO-SUNIII (BUNKOUKEIKI Co., Ltd.) and a Keithley 2400. External quantum efficiency (EQE) spectra were recorded on a SMO-250III system. The light intensity of the illumination source was adjusted by using standard silicon photodiodes: BS520 for *J–V* characteristics and SiPD S1337-1010BQ for EQE measurements, respectively.

Computation method.

DFT calculations for optimization of the geometries were conducted using the Gaussian 09 program.[1]

Synthesis.

Scheme S1

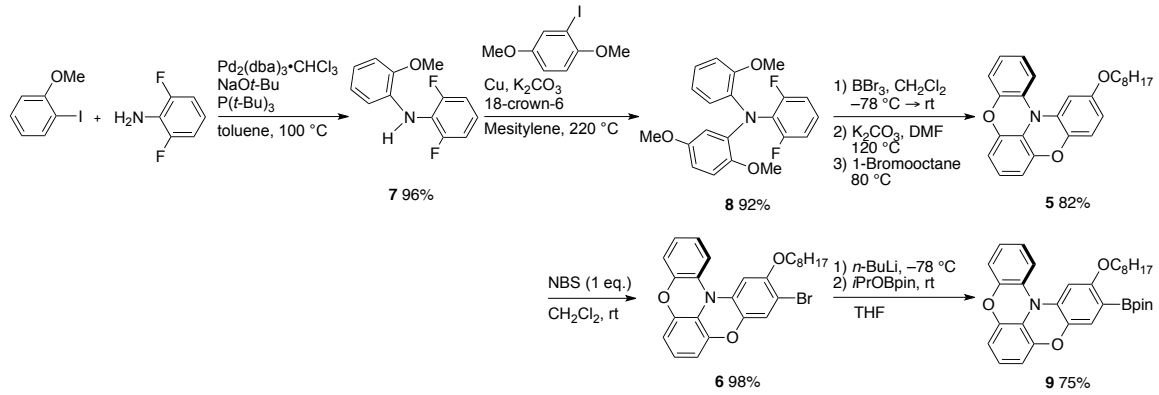

Octyloxy-substituted oxygen-bridged triarylamine derivative **5** was synthesized according to our previously reported synthetic method.[2] Using *o*-iodoanisole and 2,6-difluoroaniline as starting materials, monoarylated difluoroaniline **7** was selectively synthesized by Buchwald-Hartwig arylation in 96% yield. Subsequently, Ullmann arylation of **7** with 2-iodo-1,4-dimethoxybenzene using Cu and K_2CO_3 gave bisarylated difluoroaniline **8** in 92% yield. After cleavage of methyl groups of **8** by BBr_3, double-cyclization under the condition with K_2CO_3 in DMF at 120 °C, followed by treatment with 1-bromooctane gave **5** in 82% yield. Treatment of **5** with 1 eq. NBS selectively afforded monobrominated derivative **6** in 98% yield. Lithiation of **6** with *n*-BuLi, followed by treatment with *i*PrOBpin afforded **9** in 75% yield.

2,6-Difluoro-*N*-(2-methoxyphenyl)aniline (7). *o*-Iodoanisole (21.7 g, 92.5 mmol), 2,6-difluoroaniline (10.7 g, 82.7 mmol), $Pd_2(dba)_3{\cdot}CHCl_3$ (1.60 g, 1.59 mmol), sodium *tert*-butoxide (9.22 g, 95.9 mmol) and tri-*tert*-butylphosphine (2.58 g, 12.7 mmol) were dissolved in dry toluene (200 mL) and the mixture was stirred at 100 °C for 16 h. The insoluble materials were filtered off, and the solids were washed with toluene (150 mL). After

addition of water to the filtrate, the aqueous phase was extracted with toluene (50 mL × 3). The combined organic phase was dried over Na_2SO_4, filtered off, and concentrated under reduced pressure. The obtained crude product was passed through a short pad of silica gel with the eluent of a mixture of CH_2Cl_2 and hexane (CH_2Cl_2 : hexane = 1 : 2 , R_f = 0.45), and then purified by silica gel column chromatography (CH_2Cl_2 : hexane = 1 : 4 , R_f = 0.25) to give 18.7 g (79.4 mmol) of **7** in 96% yields as orange oil.

^{1}H NMR (500 MHz, $CDCl_3$): δ 7.18–7.01 (m, 1H), 7.18–6.93 (m, 2H), 6.91–6.81 (m, 3H), 6.60 (ddd, ^3J(H,H) = 9.0 Hz, ^3J(H,H) = 7.0 Hz, ^4J(H,H) = 2.5 Hz, 1H), 5.88 (s, 1H), 3.93 (s, 3H); ^{13}C NMR (125 MHz, $CDCl_3$): δ 157.1 (dd, ^1J(C,F) = 246.1 Hz, ^3J(C,F) = 5.7 Hz), 147.6, 133.2, 123.6 (t, ^3J(C,F) = 9.8 Hz), 120.7, 119.7, 119.0 (t, ^2J(C,F) = 15.5 Hz), 112.9 (t, ^4J(C,F) = 2.3 Hz), 111.8 (dd, ^2J(C,F) = 16.6 Hz, ^4J(C,F) = 6.8 Hz), 110.0, 55.5; HRMS(FAB) (*m/z*): $[M]^+$ calcd. for $C_{13}H_{11}F_2NO$: 235.0809; found, 235.0811; Elemental analysis calcd (%) for $C_{13}H_{11}F_2NO$: C 66.38, H 4.71, N 5.95; found: C 66.27, H 4.53, N 6.06.

2,6-Difluoro-*N*-(2,5-dimethoxyphenyl)-*N*-(2-methoxyphenyl)aniline (8). The mixture of **7** (23.3 g, 99.0 mmol), 2-iodo-1,4-dimetoxylbenzene (28.8 g, 109 mmol), K_2CO_3 (34.6 g, 250 mmol), copper powder (12.7 g, 200 mmol), and 18-crown-6 (1.28 g, 4.86 mmol) was dissolved in mesitylene (150 mL). The mixture was stirred at 220 °C for 30 h. The resulting insoluble materials were filtered off, and the solids were washed with CH_2Cl_2 (250 mL). The combined filtrate was concentrated under reduced pressure. The obtained crude product was washed with hexane (250 mL) and methanol (100 mL) to give 33.9 g (91.3 mmol) of **8** in 92% yield as white solids.

mp: 152.6–153.6 °C; ^{1}H NMR (500 MHz, $CDCl_3$): δ 7.07 (td, ^3J(H,H) = 7.5 Hz, ^4J(H,H) = 1.5 Hz, 1H), 7.01 (tt, ^3J(H,H) = 8.0 Hz, ^3J(H,F) = 6.0 Hz, 1H), 6.97 (dd, ^3J(H,H) = 7.5 Hz, ^4J(H,H) = 1.5 Hz, 1H), 6.90 (dd, ^3J(H,H) = 8.0 Hz, ^4J(H,H) = 1.0 Hz, 1H), 6.87 (td, ^3J(H,H) = 7.5 Hz, ^4J(H,H) = 1.5 Hz, 1H), 6.84 (d, ^3J(H,H) = 6.0 Hz, 1H), 6.83–6.81 (m, 2H), 3.68 (s, 3H), 3.60 (s, 3H), 3.52 (s, 3H); ^{13}C NMR (125 MHz, CD_2Cl_2): δ 159.1 (dd, ^1J(C,F) = 249 Hz, ^3J(C,F) = 6.0 Hz), 154.4, 153.5, 147.4, 138.2, 136.3, 125.0, 124.8 (t, ^2J(C,F) = 13.1 Hz), 124.7, 124.1 (t, ^3J(C,F) = 9.6 Hz), 121.1, 115.3, 113.1, 111.5 (dd, ^2J(C,F) = 18.4 Hz, ^4J(C,F) = 5.4

Hz), 110.5, 107.8, 57.3, 56.1, 55.5; HRMS (FAB) (*m/z*): $[M]^+$ calcd. for $C_{21}H_{19}F_2NO_3$, 371.1333; found, 371.1336; Elemental analysis calcd (%) for $C_{21}H_{19}F_2NO_3$: C 67.92, H 5.16, N 3.77; found: C 67.93, H 5.16, N 3.92.

2-(Octyloxy)benzo[5,6][1,4]oxazino[2,3,4-*kl*]phenoxazine (5). 8 (6.10 g, 16.4 mmol) was dissolved in CH_2Cl_2 (180 mL). BBr_3 (5.10 mL, 53.8 mmol) was added to the solution at –78 °C. The mixture was slowly warmed up to room temperature and further stirred for 3 h. The reaction mixture was poured into water and extracted with ethyl acetate (30 mL × 3). The combined organic phase was dried over Na_2SO_4, filtered off, and concentrated under reduced pressure to give 6.37 g of the crude product as white solids, which was used without further purification.

These solids were dissolved in DMF (150 mL). After addition of K_2CO_3 (9.13 g, 66.1 mmol), the mixture was stirred at 120 °C for 14 h. After the solution was cooled to room temperature, 1-bromooctane (5.30 mL, 24.7 mmol) was added. The solution was further stirred at 80 °C for 8 h. The resulting insoluble materials were filtered off, and the filtrate was concentrated under reduced pressure. The obtained solids were dissolved in CH_2Cl_2 (30 mL). After addition of water, the mixture was extracted with CH_2Cl_2 (20 mL × 3). The organic phase was dried over Na_2SO_4, filtered off, and concentrated under reduced pressure. The obtained crude product was dissolved in CH_2Cl_2. After passed through a short pad of silica gel, the crude product was purified by silica gel column chromatography (CH_2Cl_2 : hexane = 1 : 10 , R_f = 0.40) to give 5.42 g (13.5 mmol) of **5** in 82% yield as colorless oil.

^{1}H NMR (500 MHz, CD_2Cl_2): δ 7.36 (d, ^3J(H,H) = 8.0 Hz, 1H), 6.97 (td, ^3J(H,H) = 8.0 Hz, ^4J(H,H) = 2.0 Hz, 1H), 6.94–6.88 (m, 3H), 6.81 (d, ^3J(H,H) = 9.0 Hz, 1H), 6.77 (t, ^3J(H,H) = 8.0 Hz, 1H), 6.49 (d, ^3J(H,H) = 9.0 Hz, 2H), 6.42 (dd, ^3J(H,H) = 9.0 Hz, ^4J(H,H) = 2.5 Hz, 1H), 3.88 (t, ^3J(H,H) = 7.0 Hz, 2H), 1.73 (quin, ^3J(H,H) = 7.5 Hz, 2H), 1.43 (quin, ^3J(H,H) = 7.5 Hz, 2H), 1.37–1.23 (m, 8H), 0.88 (t, ^3J(H,H) = 7.0 Hz, 3H); ^{13}C NMR (125 MHz, CD_2Cl_2): δ 155.9, 147.4, 146.1, 145.7, 141.0, 130.0, 129.3, 124.06, 124.02, 123.8, 120.9, 117.73, 117.69, 115.4, 111.3, 111.1, 108.3, 102.3, 69.0, 32.2, 29.8, 29.68, 29.66, 26.4, 23.1, 14.3; HRMS (FAB) (*m/z*): $[M]^+$ calcd. for $C_{26}H_{27}NO_3$, 401.1991; found, 401.1990; Elemental analysis calcd

(%) for $C_{26}H_{27}NO_3$: C 77.78, H 6.78, N 3.49; found: C 77.57, H 6.68, N 3.75.

3-Bromo-2-(octyloxy)benzo[5,6][1,4]oxazino[2,3,4-*kl*]phenoxazine (6). 5 (4.28 g, 10.7 mmol) was dissolved in CH_2Cl_2 (160 mL). *N*-Bromosuccinimide (1.90 g, 10.7 mmol) was added to the solution and the solution was stirred at room temperature for 14 h. The reaction mixture was passed through a short pad of silica gel with an eluent of CH_2Cl_2 to give 5.00 g (10.4 mmol) of **6** in 98% yield as white solids.

mp: 65.6–66.6 °C; ^{1}H NMR (500 MHz, CD_2Cl_2): δ 7.29 (d, ^3J(H,H) = 8.0 Hz, 1H), 7.06 (s, 1H), 6.98 (dd, ^3J(H,H) = 7.5 Hz, ^4J(H,H) = 1.5 Hz, 1H), 6.97–6.88 (m, 3H), 6.77 (t, ^3J(H,H) = 8.0 Hz, 1H), 6.50 (d, ^3J(H,H) = 8.5 Hz, 1H), 6.48 (d, ^3J(H,H) = 8.5 Hz, 1H), 3.89 (t, ^3J(H,H) = 6.5 Hz, 2H), 1.78 (quin, ^3J(H,H) = 7.0 Hz, 2H), 1.47 (quin, ^3J(H,H) = 6.5 Hz, 2H), 1.40–1.23 (m, 8H), 0.90 (t, ^3J(H,H) = 7.5 Hz, 3H); ^{13}C NMR (125 MHz, CD_2Cl_2): δ 152.1, 147.4, 145.8, 145.7, 141.2, 129.3, 129.0, 124.3, 124.13, 124.05, 121.6, 120.6, 117.9, 115.0, 111.46, 111.42, 104.1, 101.0, 70.5, 32.2, 29.7, 29.6, 29.5, 26.3, 23.0, 14.3; HRMS (FAB) (*m/z*): $[M]^+$ calcd. for $C_{26}H_{26}BrNO_3$, 481.1079; found, 481.1083; Elemental analysis calcd (%) for $C_{26}H_{26}BrNO_3$: C 65.00, H 5.46, N 2.92; found: C 64.89, H 5.44, N 2.94.

2-(Octyloxy)-3-(4,4,5,5-tetramethyl-1,3,2-dioxaborolan-2-yl)benzo[5,6][1,4]oxazino[2,3,4-*kl*]phenoxazine (9). 6 (961 mg, 2.00 mmol) was dissolved in THF (40 mL) and the solution was cooled to –78 °C. *n*-BuLi in hexane (850 μL, 2.21 mmol) was added dropwise to the solution and the mixture was stirred at –78 °C for 1 h. After addition of *i*PrOBpin (450 μL, 2.21 mmol), the mixture was slowly warmed up to room temperature and further stirred for 2 h. The reaction mixture was concentrated under reduced pressure. The obtained solids were dissolved in CH_2Cl_2 (30 mL). After addition of water (30 mL), organic phase was extracted with CH_2Cl_2 (20 mL × 3). The organic phase was dried over Na_2SO_4, filtered off, and concentrated under reduced pressure. The obtained crude products were purified by gel permeation chromatography (eluent: toluene) to give 797 mg (1.51 mmol) of **9** in 75% yield as colorless oil.

^{1}H NMR (500 MHz, CD_2Cl_2): δ 7.35 (dd, ^3J(H,H) = 8.5 Hz, ^4J(H,H) = 1.5 Hz, 1H), 7.15 (s,

1H), 6.99 (td, ^{3}J(H,H) = 7.5 Hz, ^{4}J(H,H) = 1.5 Hz, 1H), 6.96–6.90 (m, 2H), 6.86 (s, 1H), 6.78 (t, ^{3}J(H,H) = 8.5 Hz, 1H), 6.50 (dd, ^{3}J(H,H) = 8.5 Hz, ^{4}J(H,H) = 1.5 Hz, 2H), 3.85 (t, ^{3}J(H,H) = 6.5 Hz, 2H), 1.74 (quin, ^{3}J(H,H) = 6.0 Hz, 2H), 1.51 (quin, ^{3}J(H,H) = 7.5 Hz, 2H), 1.37–1.26 (m, 20H), 0.89 (t, ^{3}J(H,H) = 7.0 Hz, 3H); ^{13}C NMR (125 MHz, CD_2Cl_2): δ 161.2, 147.5, 146.3, 145.6, 140.5, 132.7, 129.0, 124.5, 124.3, 124.1, 120.7, 117.8, 115.6, 111.4, 111.1, 100.0, 83.6, 70.0, 32.3, 29.8, 29.7, 26.4, 25.0, 23.1, 14.2 (One signal for the carbon atom bonding to the boron atom was not observed due to the quadrupolar relaxation of the boron atom and one sp^3-carbon signal was overlapped); HRMS (EI) (*m/z*): $[M]^+$ calcd. for $C_{32}H_{38}BNO_5$, 527.2849; found, 527.2852; Elemental analysis calcd (%) for $C_{32}H_{38}BNO_5$: C 72.87, H 7.26, N 2.66; found: C 72.78, H 7.17, N 2.71.

1,3,5,7-Tetra(Bpin)azulene was synthesized by direct borylation using Ir catalyst, according to our previous report.[3] 5,7-Di(Bpin)azulene was obtained by the selective deborylation of 1,3,5,7-tetra(Bpin)azulene.[3] Tetra-substituted derivative **1** was obtained by Suzuki-Miyaura cross coupling of the brominated derivative **6** and 1,3,5,7-tetra(Bpin)azulene in 58% yield as green solids. In a similar manner, coupling reaction of **6** and 5,7-di(Bpin)azulene afforded the derivative **3** in 76% yield as green solids.

1,3-dibromoazulene was obtained by bromination of azulene with 2 eq. of NBS in 79% yield.[4] Suzuki-Miyaura cross coupling of 1,3-dibromoazulene and the borylated derivative **9** afforded **2** in 46% yield as green solids.

3,3´,5,5´-Tetra(Bpin)-1,1´-biphenyl was also prepared by selective direct borylation with Ir catalyst.[5] Suzuki-Miyaura cross coupling of 3,3´,5,5´-tetra(Bpin)-1,1´-biphenyl and **6** afforded tetra-substituted biphenyl derivative **4** in 59% yield as pale yellow solids.

Scheme S2

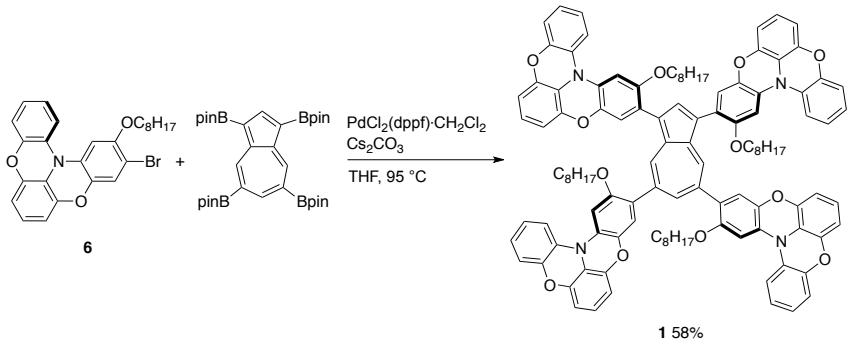

1,3,5,7-Tetrakis(2-(octyloxy)benzo[5,6][1,4]oxazino[2,3,4-*kl*]phenoxazin-3-yl)azulene (1). 1,3,5,7-Tetra(Bpin)azulene (639 mg, 1.01 mmol), **6** (2.33 g, 4.84 mmol), $PdCl_2(dppf)\cdot CH_2Cl_2$ (50.5 mg, 61.8 μmol), and cesium carbonate (3.29 g, 10.1 mmol) in THF (90 mL) were charged in a Schlenk tube. After flushed with argon three times, the mixture was stirred at 95 °C for 2 d. After passed through a short pad of silica gel with an eluent of CH_2Cl_2, the obtained crude product was further purified by silica gel column chromatography (hexane : CH_2Cl_2 = 3 : 1 , R_f = 0.20) to give 1.01 g (0.583 mmol) of **1** in 58% yield as green solids.

mp: 114.9–116.7 °C; ^{1}H NMR (500 MHz, CD_2Cl_2): δ 8.48 (s, 2H), 8.12 (s, 1H), 7.89 (s, 1H), 7.45 (d, ^3J(H,H) = 8.0 Hz, 2H), 7.41 (d, ^3J(H,H) = 8.0 Hz, 2H), 7.08 (s, 4H), 7.04–6.97 (m, 8H), 6.95–6.91 (m, 8H), 6.79 (t, ^3J(H,H) = 8.0 Hz, 2H), 6.78 (t, ^3J(H,H) = 8.0 Hz, 2H), 6.54–6.49 (m, 8H), 3.89 (t, ^3J(H,H) = 7.0 Hz, 4H), 3.83 (t, ^3J(H,H) = 7.0 Hz, 4H), 1.65 (quin, ^3J(H,H) = 7.5 Hz, 4H), 1.60 (quin, ^3J(H,H) = 7.5 Hz, 4H), 1.28–1.09 (m, 40H), 0.79 (t, ^3J(H,H) = 7.0 Hz, 6H), 0.78 (t, ^3J(H,H) = 7.0 Hz, 6H); ^{13}C NMR (125 MHz, CD_2Cl_2): δ 153.1, 152.3, 147.4, 146.0, 145.9, 145.8, 145.7, 142.4, 140.9, 140.7, 138.0, 135.8, 131.8, 129.6, 129.5, 129.3, 128.6, 127.9, 126.5, 124.15, 124.07, 123.7, 123.6, 121.6, 121.0, 120.8, 120.0, 117.78, 117.75, 115.0, 111.4, 111.2, 111.1, 101.2, 100.8, 69.94, 69.91, 32.3, 29.8, 29.74, 29.69, 29.66, 29.60, 29.5, 26.5, 26.3, 23.05, 23.03, 14.3 (seven sp^2 and two sp^3-carbon signals were overlapped); HRMS (FAB) (*m/z*): $[M]^+$ calcd. for $C_{114}H_{108}N_4O_{12}$, 1724.7964; found, 1724.7959; Elemental analysis calcd (%) for $C_{114}H_{108}N_4O_{12}$: C 79.32, H 6.31, N 3.25; found: C 79.25, H 6.26, N 3.27.

Scheme S3

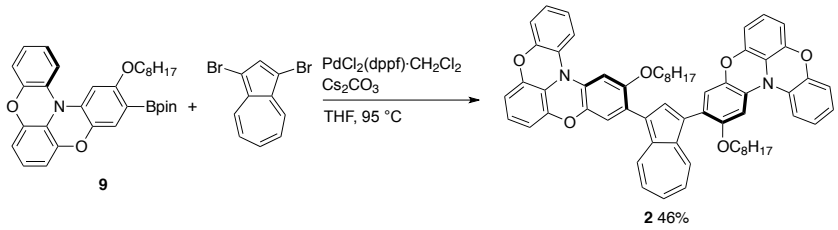

9 **2** 46%

1,3-Bis(2-(octyloxy)benzo[5,6][1,4]oxazino[2,3,4-*kl*]phenoxazin-3-yl)azulene (2). 1,3-Dibromoazulene (129 mg, 0.453 mmol), **9** (518 mg, 0.982 mmol), $PdCl_2(dppf)\cdot CH_2Cl_2$ (12.9 mg, 15.8 μmol), and cesium carbonate (739 mg, 2.27 mmol) in THF (20 mL) were charged in a Schlenk tube. After flushed with argon three times, the mixture was stirred at 95 °C for 24 h. The mixture was passed through a short pad of silica gel with an eluent of CH_2Cl_2. The obtained crude product was purified by gel permeation chromatography (eluent: toluene) and further purified by silica gel column chromatography (hexane : CH_2Cl_2 = 3 : 1 , R_f = 0.30) to give 191 mg (0.206 mmol) of **2** in 46% yield as green solids.

mp: 73.8–75.7 °C; ^{1}H NMR (500 MHz, CD_2Cl_2): δ 8.32 (d, ^3J(H,H) = 9.5 Hz, 2H), 8.11 (s, 1H), 7.58 (t, ^3J(H,H) = 9.5 Hz, 1H), 7.48 (d, ^3J(H,H) = 8.0 Hz, 2H), 7.13 (t, ^3J(H,H) = 9.5 Hz, 2H), 7.10 (s, 2H), 7.06–7.02 (m, 4H), 6.97–6.92 (m, 4H), 6.80 (t, ^3J(H,H) = 8.0 Hz, 2H), 6.54 (t, ^3J(H,H) = 8.5 Hz, 4H), 3.83 (t, ^3J(H,H) = 7.0 Hz, 4H), 1.58 (quin, ^3J(H,H) = 7.0 Hz, 4H), 1.21 (quin, ^3J(H,H) = 7.0 Hz, 4H), 1.18–1.09 (m, 16H), 0.82 (t, ^3J(H,H) = 7.0 Hz, 6H); ^{13}C NMR (125 MHz, CD_2Cl_2): δ 153.2, 147.5, 146.1, 145.8, 140.8, 140.4, 138.6, 137.2, 136.3, 129.7, 128.2, 125.7, 124.2, 123.7, 123.3, 121.6, 121.0, 120.8, 117.8, 115.1, 111.5, 111.2, 101.2, 100.8, 69.9, 32.2, 29.65, 29.63, 29.57, 26.5, 23.0, 14.2 (one sp^2-carbon signal was overlapped); HRMS (FAB) (*m/z*): $[M]^+$ calcd. for $C_{62}H_{58}N_2O_6$, 926.4295; found, 926.4301; Elemental analysis calcd (%) for $C_{62}H_{58}N_2O_6$: C 80.32, H 6.31, N 3.02; found: C 80.35, H 6.40, N 3.07.

Scheme S4

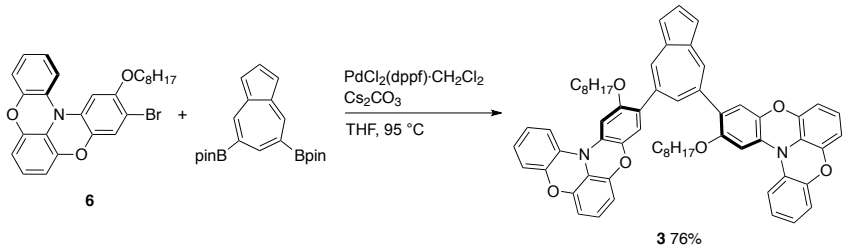

5,7-Bis(2-(octyloxy)benzo[5,6][1,4]oxazino[2,3,4-*kl*]phenoxazin-3-yl)azulene (3). 5,7-Di(Bpin)azulene (237 mg, 0.624 mmol), **6** (663 mg, 1.38 mmol), $PdCl_2(dppf)\cdot CH_2Cl_2$ (15.0 mg, 18.4 μmol), and cesium carbonate (1.04 g, 3.19 mmol) in THF (30 mL) were charged in a Schlenk tube. After flushed with argon three times, the mixture was stirred at 95 °C for 48 h. The mixture was passed through a short pad of silica gel with an eluent of CH_2Cl_2. The obtained crude product was purified by silica gel column chromatography (hexane : CH_2Cl_2 = 2 : 1 , R_f = 0.38) to give 439 mg (0.473 mmol) of **3** in 76% yield as green solids.

mp: 73.5–74.7 °C; ^{1}H NMR (500 MHz, CD_2Cl_2): δ 8.54 (d, ^4J(H,H) = 1.5 Hz, 2H), 7.92 (t, ^4J(H,H) = 1.5 Hz, 1H), 7.88 (t, ^3J(H,H) = 3.5 Hz, 1H), 7.43 (d, ^3J(H,H) = 7.5 Hz, 2H), 7.37 (d, ^3J(H,H) = 3.5 Hz, 2H), 7.04 (s, 2H), 7.05–7.00 (m, 4H), 6.96–6.92 (m, 4H), 6.79 (t, ^3J(H,H) = 8.0 Hz, 2H), 6.53 (d, ^3J(H,H) = 8.0 Hz, 2H), 6.52 (d, ^3J(H,H) = 8.0 Hz, 2H), 3.89 (t, ^3J(H,H) = 6.5 Hz, 4H), 1.65 (quin, ^3J(H,H) = 7.5 Hz, 4H), 1.31 (quin, ^3J(H,H) = 7.5 Hz, 4H), 1.25–1.12 (m, 16H), 0.82 (t, ^3J(H,H) = 7.0 Hz, 6H); ^{13}C NMR (125 MHz, CD_2Cl_2): δ 152.4, 147.5, 146.0, 145.8, 141.5, 141.0, 139.0, 138.8, 137.3, 131.5, 129.6, 129.5, 128.8, 124.24, 124.16, 123.8, 120.9, 119.9, 119.1, 117.8, 115.1, 111.4, 111.3, 100.9, 69.9, 32.2, 29.63, 29.60, 29.5, 26.4, 23.0, 14.2; HRMS (FAB) (*m/z*): $[M]^+$ calcd. for $C_{62}H_{58}N_2O_6$, 926.4295; found, 926.4300; Elemental analysis calcd (%) for $C_{62}H_{58}N_2O_6$: C 80.32, H 6.31, N 3.02; found: C 80.29, H 6.29, N 3.00.

Scheme S5

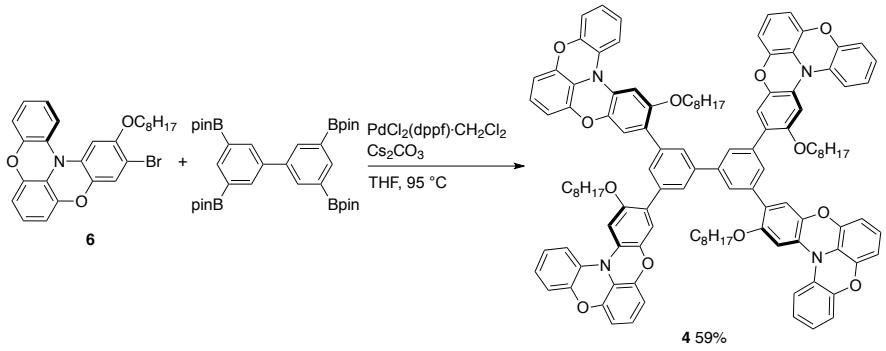

3,3´,5,5´-Tetrakis(2-(octyloxy)benzo[5,6][1,4]oxazino[2,3,4-*kl*]phenoxazin-3-yl)-1,1´-biphenyl (4). 3,3´,5,5´-Tetra(Bpin)-1,1´-biphenyl (39.5 mg, 0.601 mmol), **8** (173 mg, 0.360 mmol), $PdCl_2(dppf)\cdot CH_2Cl_2$ (10.1 mg, 12.3 μmol), and cesium carbonate (196 mg, 0.601 mmol) in THF (5 mL) were charged in a pressure vessel. After degassed for 10 min, the solution was stirred at 95 °C for 27 h. After diluted with CH_2Cl_2 (20 mL), the reaction mixture was quenched with 1 M HCl aq. The organic phase was extracted with CH_2Cl_2 (5 mL × 3), followed by washing with water and brine. The combined organic phase was dried over $MgSO_4$, filtered off, and concentrated under reduced pressure. The obtained crude product was purified by silica gel column chromatography (hexane : CH_2Cl_2 = 4 : 1 , R_f = 0.17) to give 62.3 mg (0.0355 mmol) of **4** in 59% yield as pale yellow solids.

mp: 99.8–101.6°C; ^{1}H NMR (500 MHz, CD_2Cl_2): δ 7.87 (s, 4H), 7.75 (s, 2H), 7.43 (d, ^3J(H,H) = 8.0 Hz, 4H), 7.09 (s, 4H), 7.04 (s, 4H), 7.03–6.98 (m, 4H), 6.97–6.92 (m, 8H), 6.79 (t, ^3J(H,H) = 8.0 Hz, 4H), 6.53 (d, ^3J(H,H) = 8.0 Hz, 4H), 6.52 (d, ^3J(H,H) = 8.0 Hz, 4H), 3.91 (t, ^3J(H,H) = 6.5 Hz, 8H), 1.74 (quin, ^3J(H,H) = 7.5 Hz, 8H), 1.34 (quin, ^3J(H,H) = 7.5 Hz, 8H), 1.20–1.06 (m, 32H), 0.75 (t, ^3J(H,H) = 7.0 Hz, 12H); ^{13}C NMR (125 MHz, CD_2Cl_2): δ 152.7, 147.5, 146.0, 145.8, 141.1, 140.9, 138.1, 129.54, 129.48, 128.8, 127.1, 125.7, 124.2, 124.1, 123.8, 120.9, 119.3, 117.8, 115.1, 111.5, 111.2, 100.8, 69.9, 32.3, 29.78, 29.71, 29.5, 26.6, 23.0, 14.2; HRMS (FAB) (*m/z*): $[M]^+$ calcd. for $C_{116}H_{110}N_4O_{12}$, 1750.8120; found, 1750.8118; Elemental analysis calcd (%) for $C_{116}H_{110}N_4O_{12}$: C 79.52, H 6.33, N 3.20; found: C 79.15, H 6.63, N 3.05.

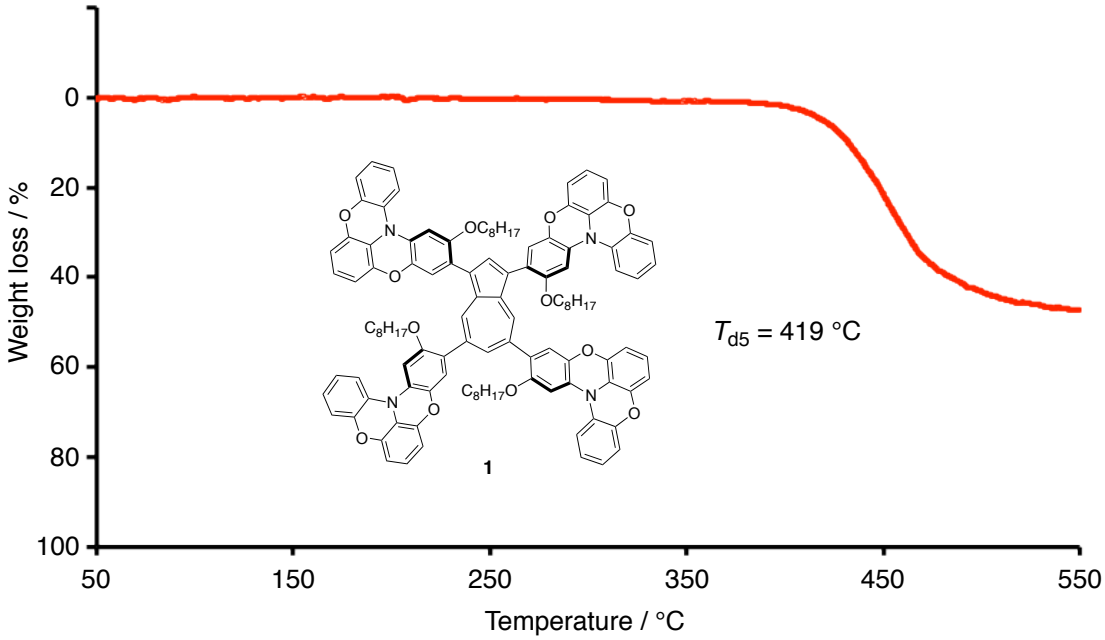

Figure S1. Thermogravimetric analysis of **1** heating at 10 °C/min under N_2.

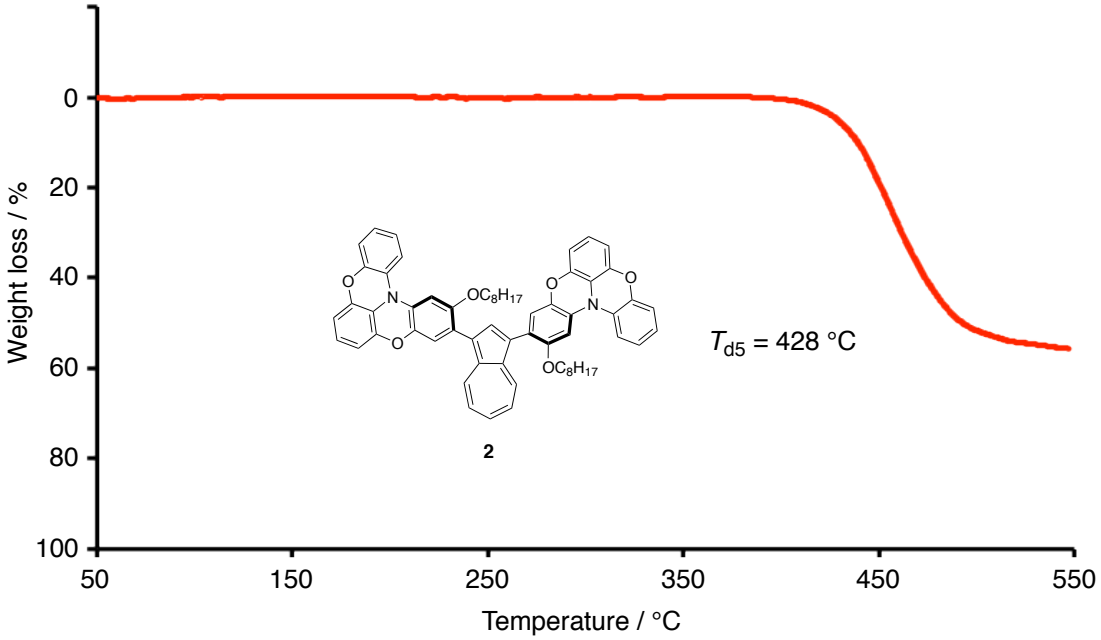

Figure S2. Thermogravimetric analysis of **2** heating at 10 °C/min under N_2.

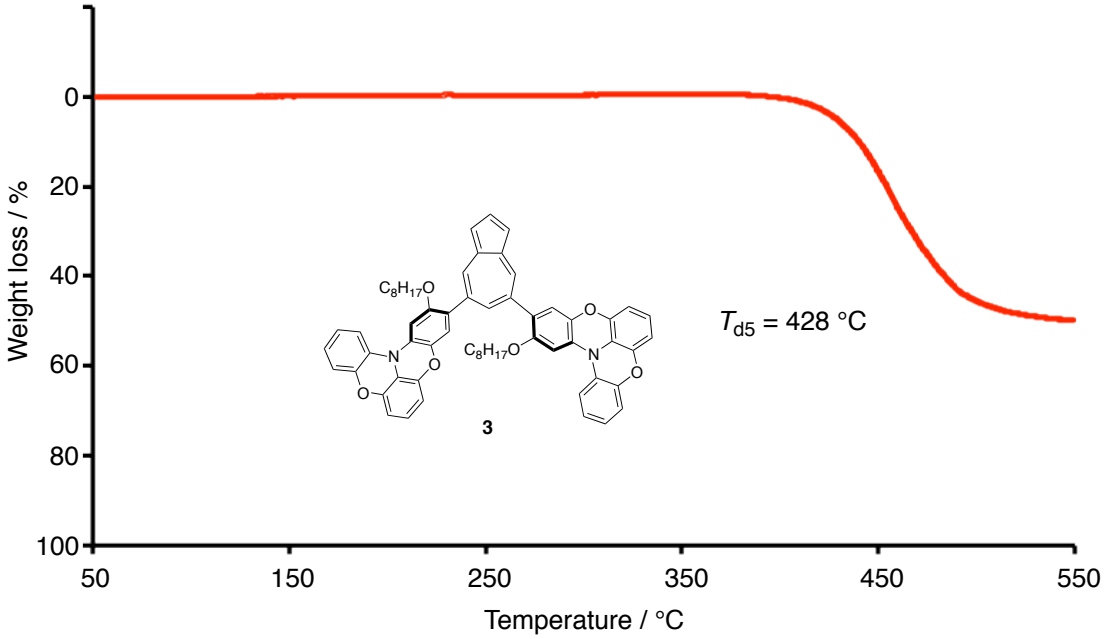

Figure S3. Thermogravimetric analysis of **3** heating at 10 °C/min under N_2.

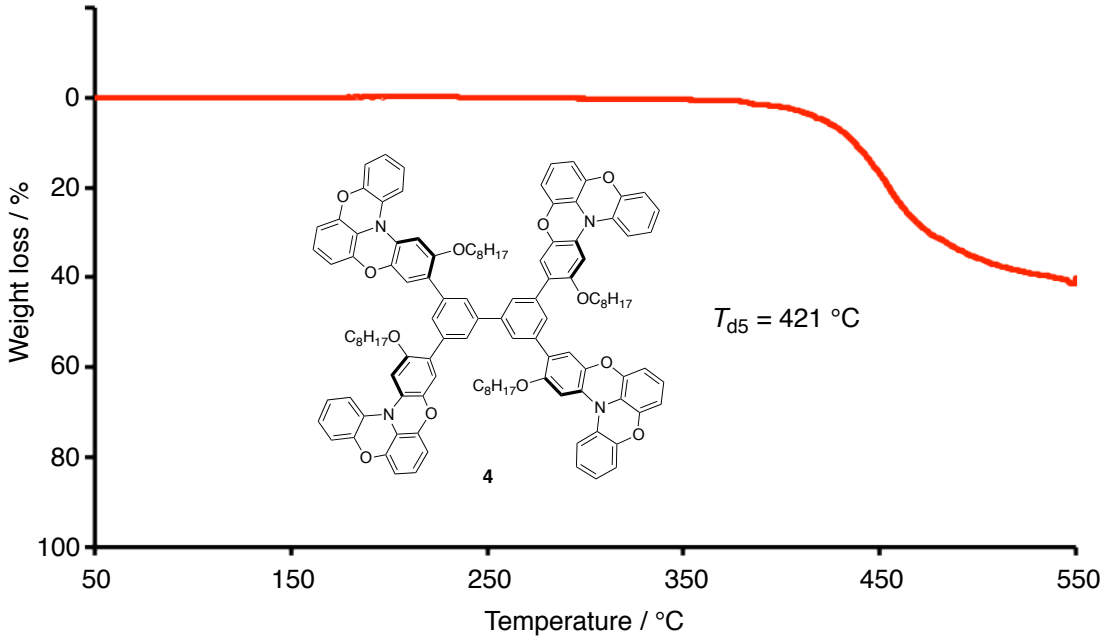

Figure S4. Thermogravimetric analysis of **4** heating at 10 °C/min under N_2.

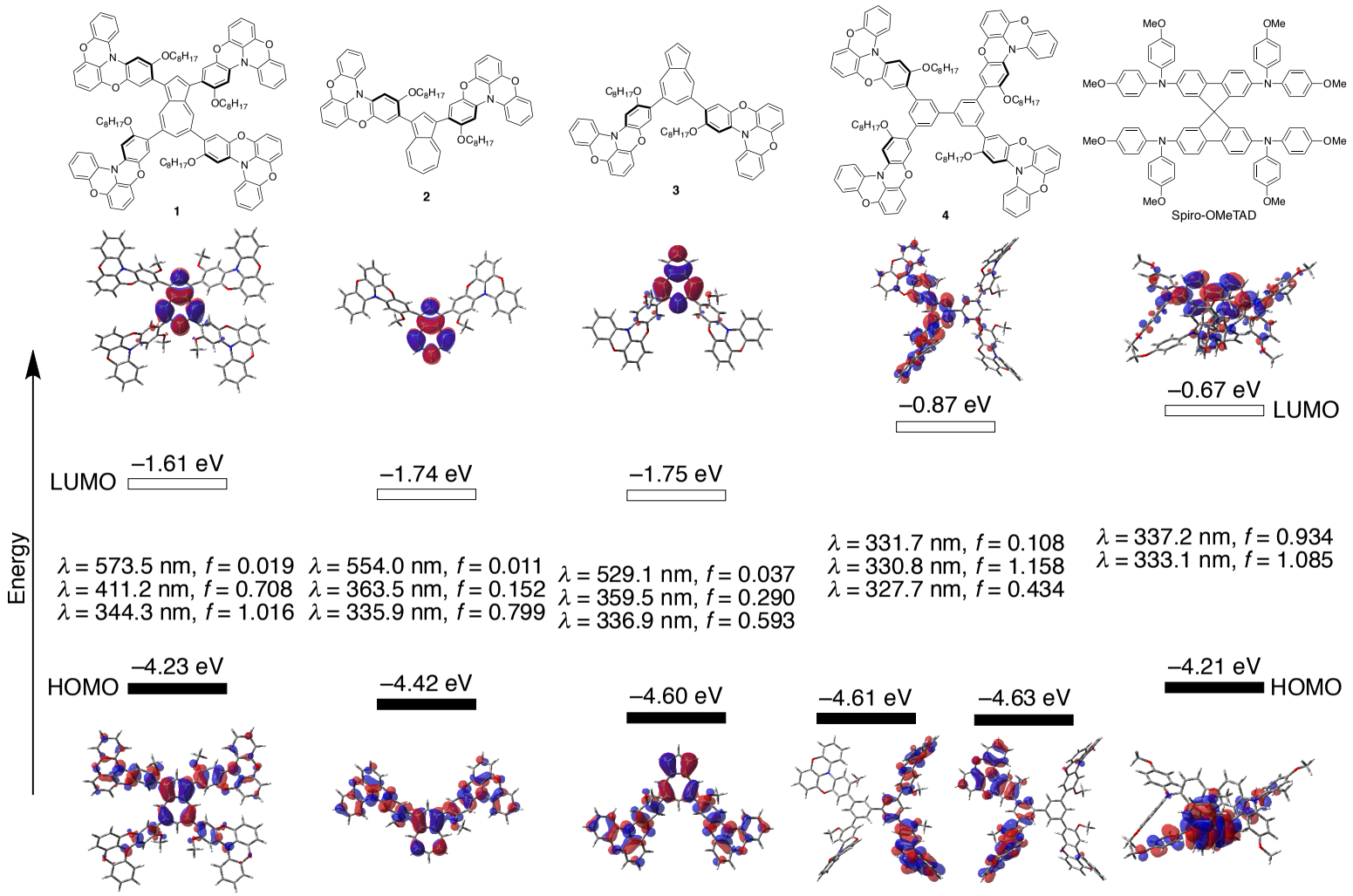

Figure S5. Pictorial presentation of the frontier orbitals, a plot of the Kohn-Sham HOMO and LUMO energy levels for **1–4** and Spiro-OMeTAD (B3LYP/6-31G(d)), and optical transition with oscillator strength (CAM-B3LYP/6-31G(d)//B3LYP/6-31G(d)).

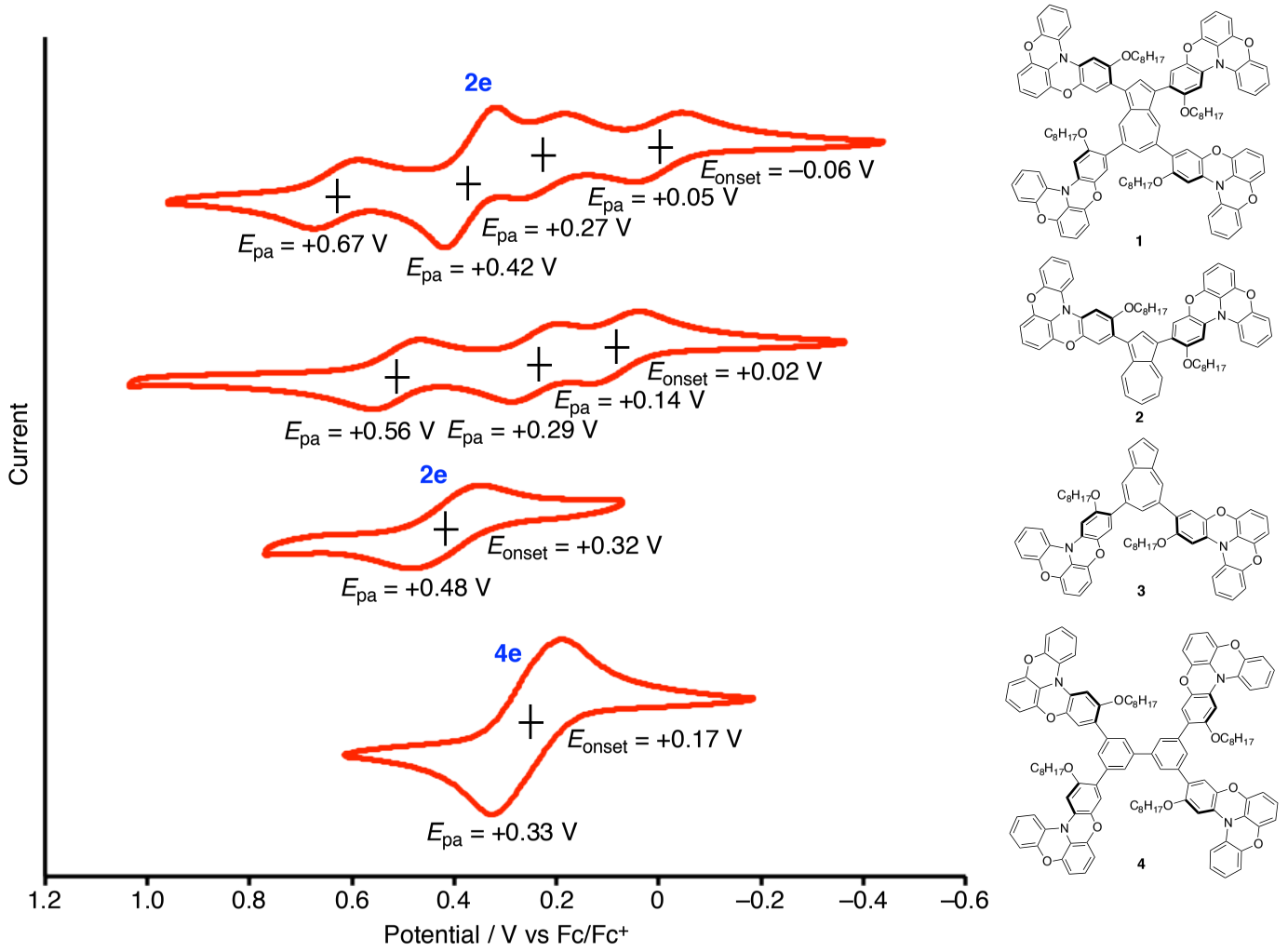

Figure S6. Cyclic voltammograms of **1–4** in CH_2Cl_2 (0.5 mM), measured with $(n\text{-Bu})_4N^+PF_6^-$ as a supporting electrolyte at a scan rate of 100 mVs^{-1}.

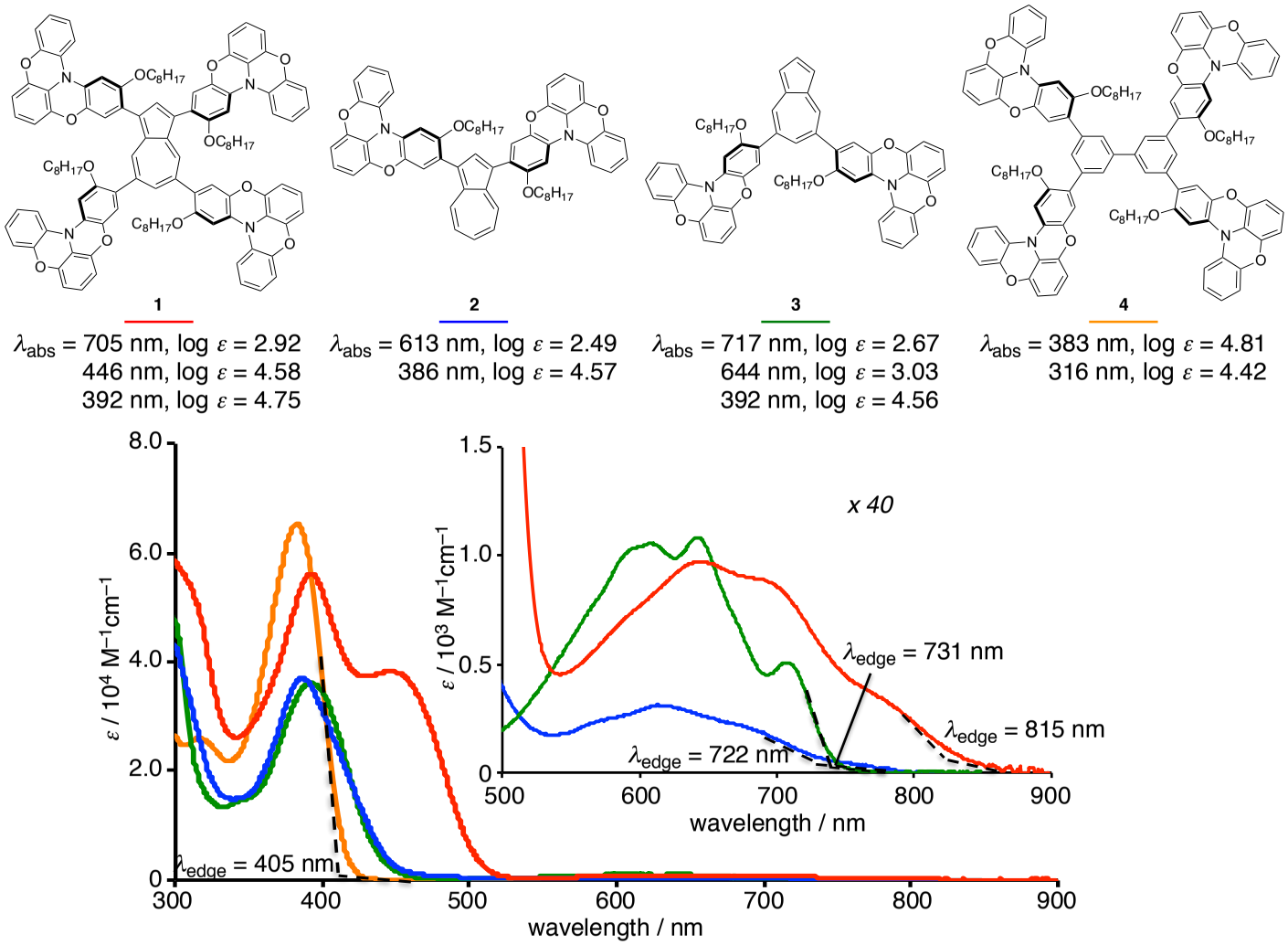

Figure S7. UV-vis absorption spectra of **1–4** in CH_2Cl_2.

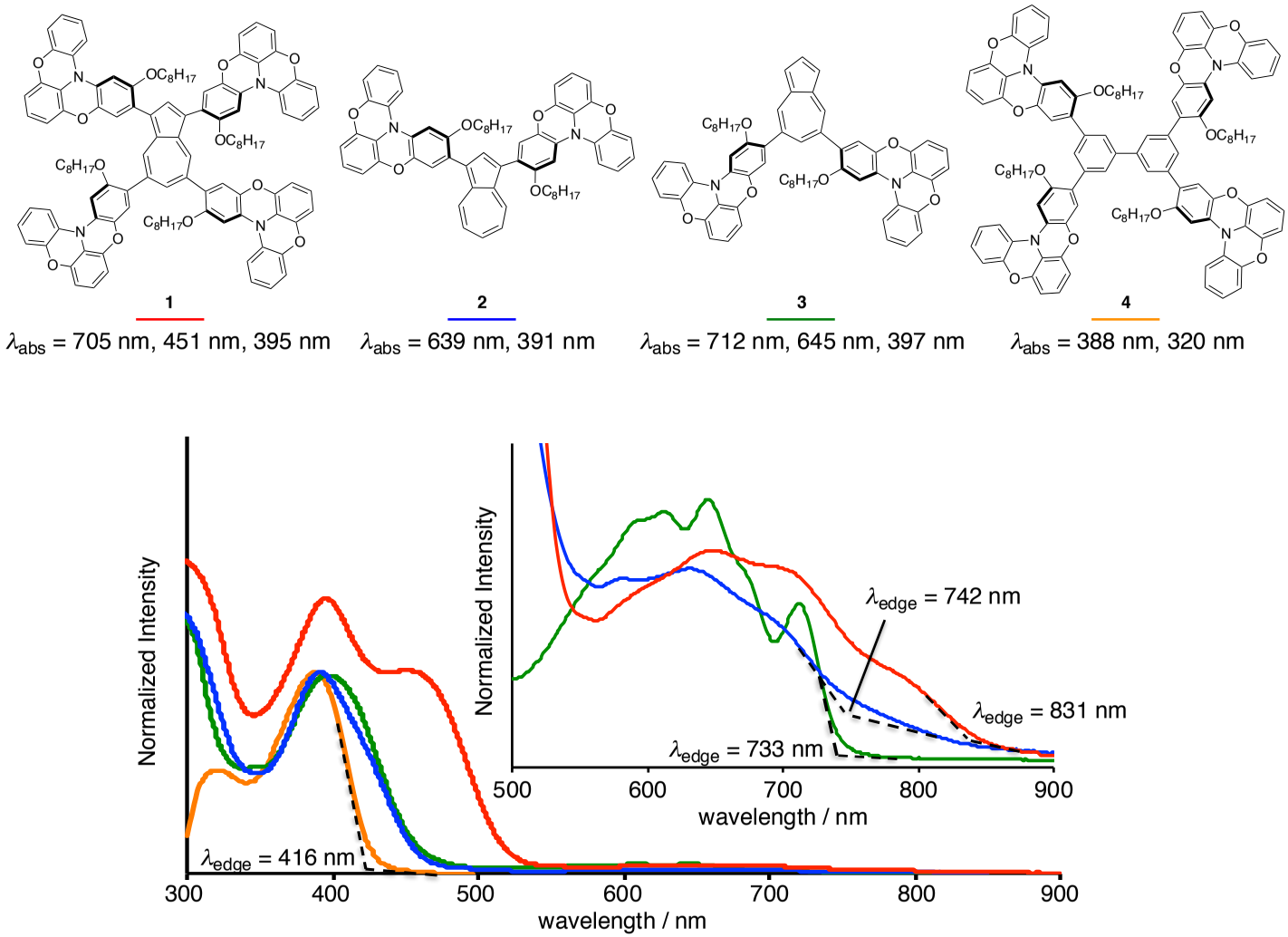

Figure S8. UV-vis absorption spectra of **1–4** in the spin-coated films.

Peovskite Solar cells: Device fabrication.

1) Preparation of mesoporous TiO_2 layer

Patterned transparent conducting oxide substrate (FTO, 25 mm × 25 mm, Asahi Glass Co., Ltd., Japan) was treated with ultrasonic cleaning for 10 min with a 1wt% neutral aqueous detergent solution, acetone, 2-propanol, and distilled water, respectively, and then subjected to an O_3/ultraviolet treatment for 15 min.

FTO substrate was covered with a compact TiO_2 layer by spray pyrolysis of a ethanol solution (0.05 M) of titanium di-isopropoxide bis(acetylacetonate) (75wt% in 2-propanol, Tokyo Chemical Industry Co., Ltd., Japan) at 450 °C. The resulting compact TiO_2 layer was treated with an aqueous solution (100 mL) of $TiCl_4$ (440 μL, special grade, Wako Pure Chemical Industries Ltd., Japan) at 70 °C for 30 min, followed by rinsing twice with distilled water. The substrate was sintered at 500 °C for 20 min.

Subsequently, mesoporous-TiO_2 layer (thickness: 200 nm; average particle size: ca. 20 nm) was deposited on the plate by spin-coating (slope 5 s, 5000 rpm, 30 s, slope 5 s) of a suspension of TiO_2 paste (PST–18NR, JGC Catalysts and Chemicals Ltd.) in ethanol (paste : ethanol = 1 : 5 wt ratio), followed by sintering at 500 °C for 30 min.

The obtained substrate was treated with ultraviolet-ozone cleaning for 15 min before used for perovskite layer fabrication.

2-A) Two-step solution method for perovskite layer

In a glove box filled with an inert gas, a 1.0 M solution of PbI_2 (L0279 for perovskite precursor, Tokyo Chemical Industry Co., Ltd., Japan) in dehydrated DMF at 70 °C was deposited on the mesoporous TiO_2 films by spin-coating (slope 5 s, 6500 rpm, 5 s, slope 5 s). The resulting yellow film was annealed on a hot plate at 70 °C for 1 h. The film was dipped in a 0.06 M 2-propanol solution of CH_3NH_3I (Tokyo Chemical Industry Co., Ltd., Japan) for 40 s. The formed perovskite film was then annealed on a hot plate at 70 °C for 1 h.

2-B) One-step solution method using toluene dropping for perovskite layer

In a glove box filled with an inert gas, a 1.1 M solution of PbI_2 and CH_3NH_3I in DMSO (room temperature) was deposited on the mesoporous TiO_2 films by spin-coating (slope 1 s, 1000 rpm 40 s, slope 1 s, 0 rpm. 30 s, slope 5 s, 5000 rpm 20 s, slope 5 s: At the last 5 s of spin-coating, 0.5 mL of toluene was slowly dropped on the rotating substrate.). The resulting transparent film was annealed on a hot plate at 100 °C for 10 min to form perovskite layer (250 nm).

3) Preparation of hole-transporting layer and Au electrode

A mixture of hole-transporting material (**HTM**, 0.050 M) and [tris(2-(1*H*-pyrazol-1-yl)-4-*tert*-butylpyridine)cobalt(III) tris(bis(trifluoromethylsulfonyl)imide)][6] (FK209, 0–15.0 mg, 0−0.010 M (for 0.0 eq. –0.20 eq.)) as an oxidizing agent was dissolved with a solution containing chlorobenzene (1 mL), 4-*tert*-butylpyridine (TBP, 24.4 μL, 0.165 M, Aldrich), and lithium bis(trifluoromethylsulfonyl)imide (LITFSI, 7.6 mg, 0.027 M, Wako Pure Chemical Industries Co., Ltd.). After 30 min, the resulting suspension was filtered with a membrane filter (Cosmonice filter S, Nacarai Tesque, Inc.) in order to remove the formed insoluble Co(II) complex. The hole-transporting layer was deposited on the perovskite layer by spin-coating (slope 5 s, 4000 rpm, 30 s, slope 5 s) of the obtained filtrate. The resulting film was dried on a hot plate (at 40 °C for **1**–**4**, and at 70 °C for Spiro-OMeTAD, respectively) for 30 min. Finally, a gold layer (80 nm) was thermally deposited on the hole-transporting layer.

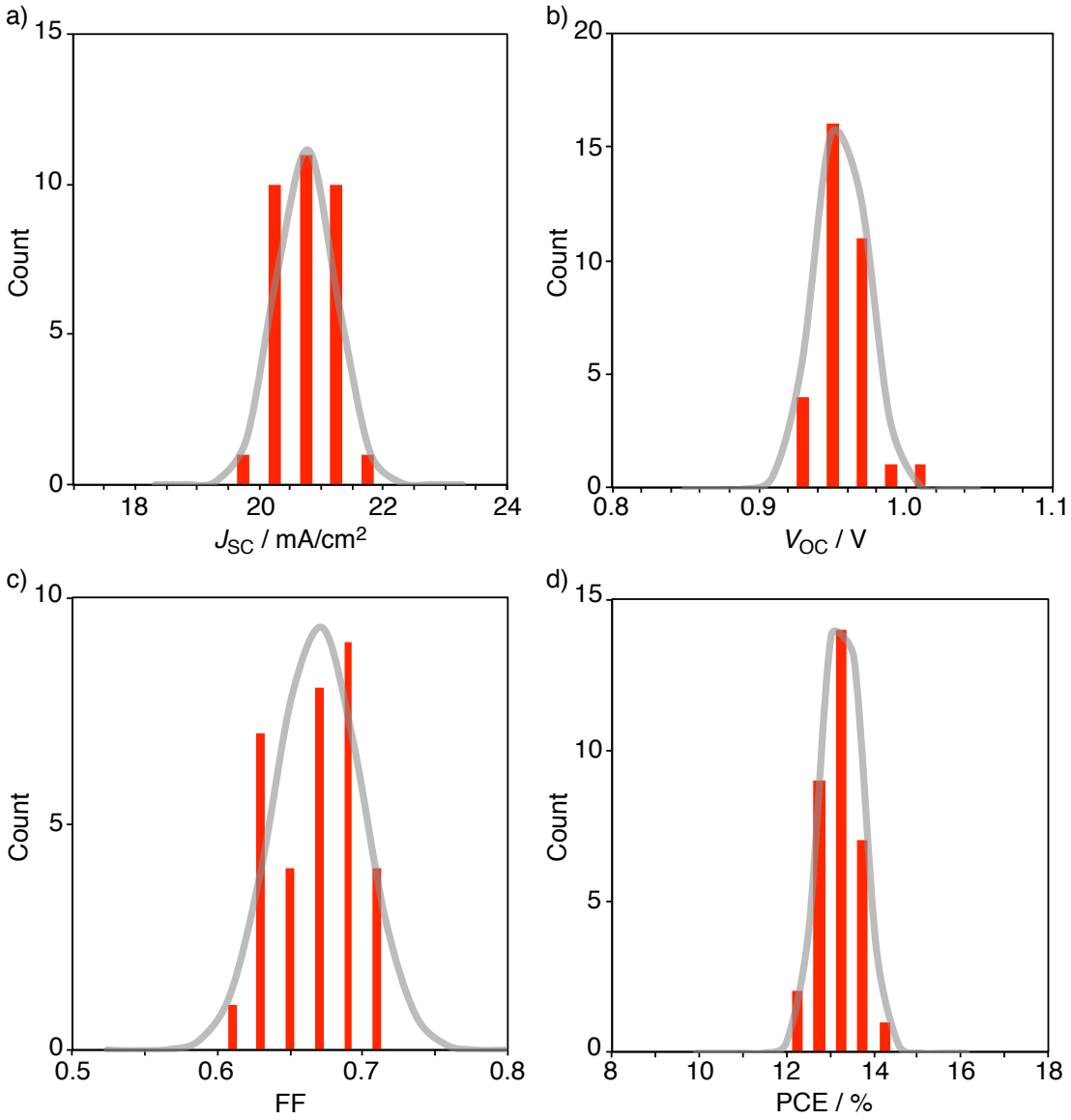

Figure S9. Histograms of each value of (a) J_{SC}, (b) V_{OC}, (c) FF and (d) PCE for 33 samples of perovskite solar cells (0.04 cm^2 mask), which were prepared by optimum two-step solution method for perovskite layer using Spiro-OMeTAD with 0.10 eq. Co (III) dopant as a HTM.

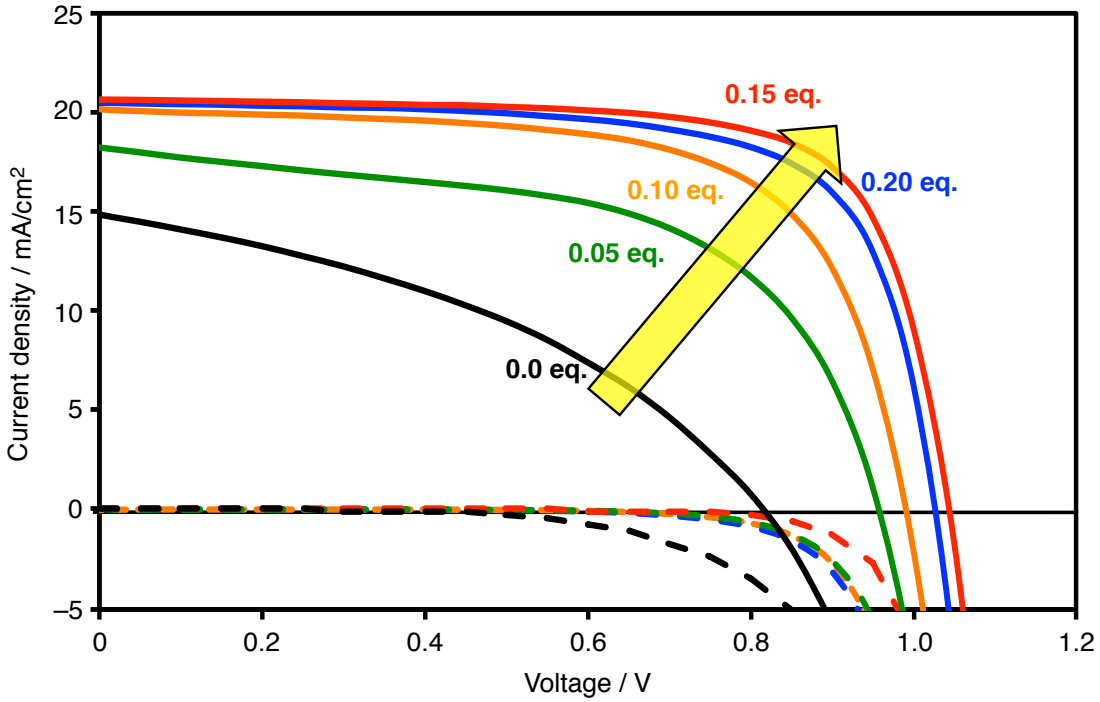

Figure S10. Current density-voltage characteristics of perovskite solar cells using **1** with different amount of Co(III) dopant (0.0 eq.: black, 0.05 eq.: green, 0.10 eq.: orange, 0.15 eq.: red, 0.20 eq.: blue) measured with a mask (0.04 cm^2) under 100 nW/cm^2 photon flux (AM1.5G) (solid line) and dark condition (dashed line).

Table S1. Summary of Photovoltaic Parameters Derived from *J–V* Measurements of Perovskite Solar Cells using 1

Co(III) Dopant [eq.]	J_{SC} [mA/cm^2]	V_{OC} [V]	FF	PCE [%]	R_s [Ωcm^2]	R_{sh} [Ωcm^2]
0.0	14.9	0.82	0.39	4.8	15	1.2×10^2
0.05	18.2	0.96	0.57	9.9	6.8	2.1×10^2
0.10	20.1	0.99	0.66	13.2	7.0	7.4×10^2
0.15	20.7	1.04	0.73	15.7	8.6	1.6×10^3
0.20	20.5	1.02	0.71	14.8	6.8	1.6×10^3

Components in the solution for the deposition of hole-transporting layer: **1** (0.050 M), FK209 (0.0–0.010 M), TBP (0.165 M), and LiTFSI (0.027 M) in chlorobenzene.

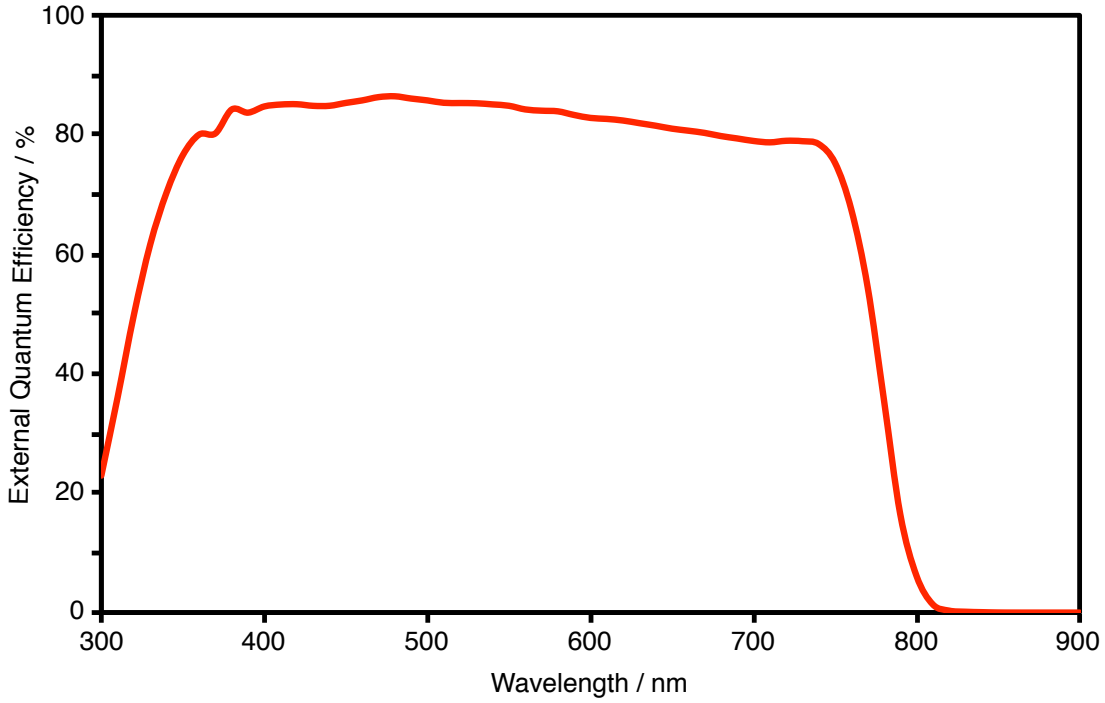

Figure S11. External quantum efficiency spectrum for perovskite solar cell (0.04 cm^2 mask) using **1** with 0.15 eq. Co (III) dopant, in which perovskite layer was fabricated by two-step solution method.

As shown in Figure S12, the cell using **1** showed moderate hysteresis behavior, in which the forward scan performs better than the reverse scan. This hysteresis behavior is diametrally opposed to that observed in cells using Spiro-OMeTAD (Figure S13). The origin of this moderate hysteresis remains unclear at present.

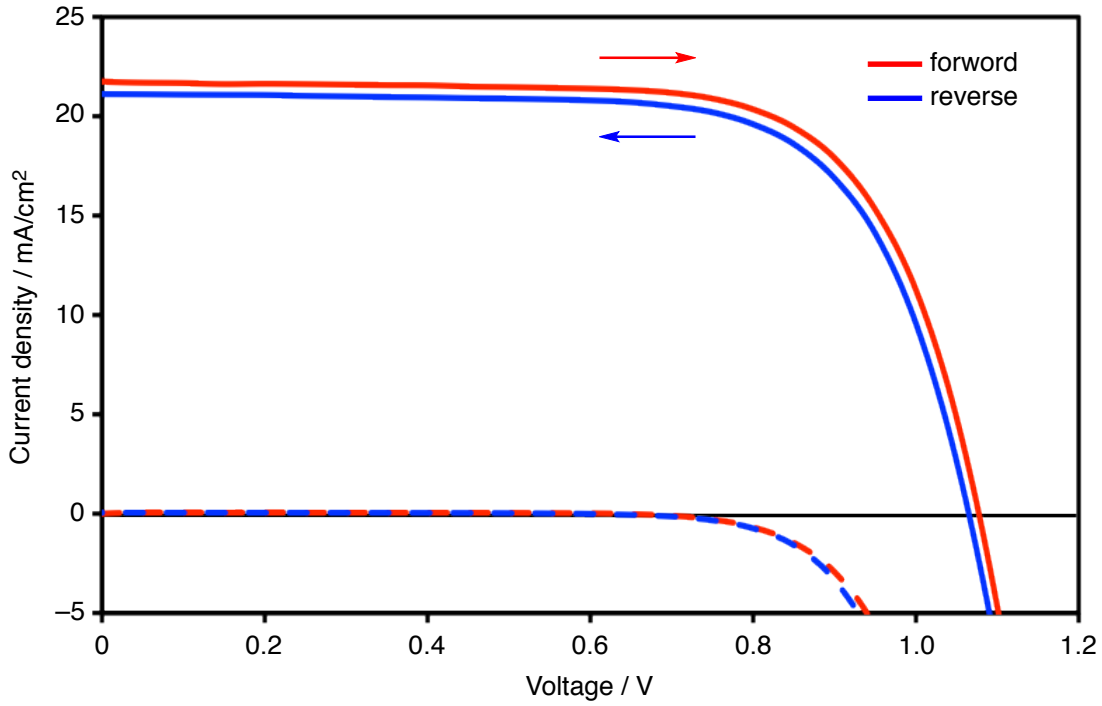

Figure S12. Current density-voltage characteristics of perovskite solar cells using **1**, in which perovskite layer was fabricated by one-step solution method, measured by forward (red) and reverse (blue) scans with a mask (0.10 cm^2) under 100 nW/cm^2 photon flux (AM1.5G) (solid line) and dark condition (dashed line).

Table S2. Summary of Photovoltaic Parameters Derived from *J–V* Measurements of Perovskite Solar Cells using 1, in which Perovskite Layer was Fabricated by One-Step Solution Method

Scan Direction	J_{SC} [mA/cm^2]	V_{OC} [V]	FF	PCE [%]	R_s [Ωcm^2]	R_{sh} [Ωcm^2]
Forward	21.7	1.08	0.71	16.5	6.9	1.9×10^3
Reverse	21.1	1.06	0.70	15.8	7.7	2.4×10^3

Components in the solution for the deposition of hole-transporting layer: **1** (0.050 M), FK209 (0.0–0.010 M), TBP (0.165 M), and LiTFSI (0.027 M) in chlorobenzene.

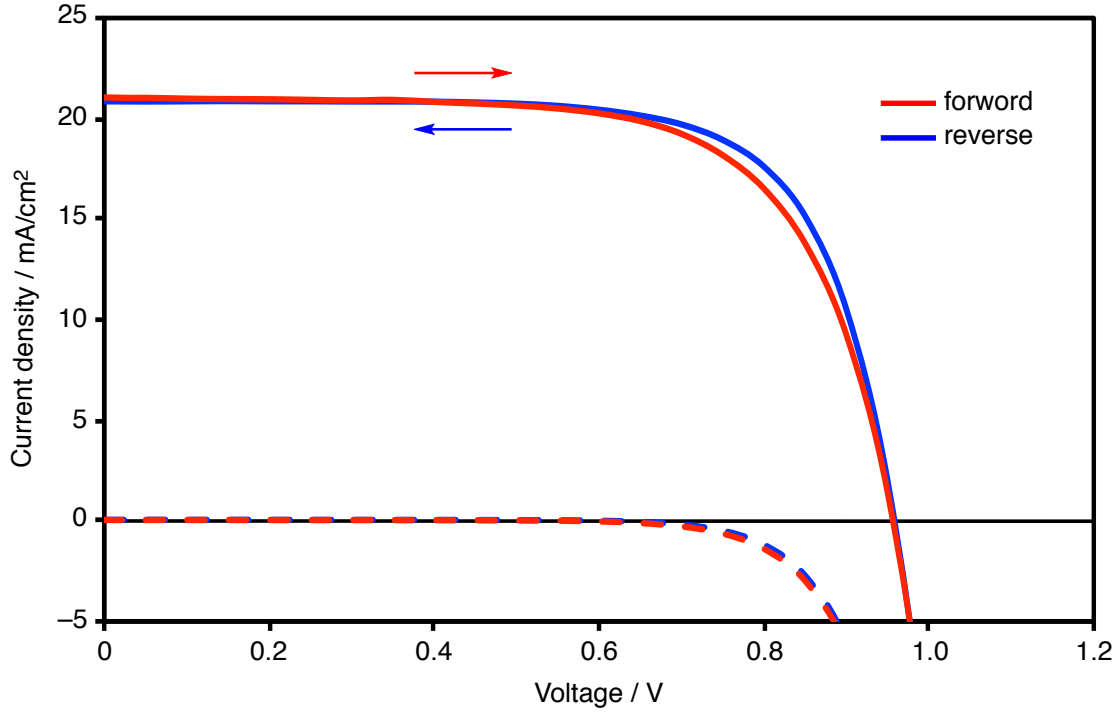

Figure S13. Current density-voltage characteristics of perovskite solar cells using Spiro-OMeTAD, in which perovskite layer was fabricated by two-step solution method, measured by forward (red) and reverse (blue) scans with a mask (0.04 cm^2) under 100 nW/cm^2 photon flux (AM1.5G) (solid line) and dark condition (dashed line).

Table S3. Summary of Photovoltaic Parameters Derived from *J–V* Measurements of Perovskite Solar Cells using Spiro-OMeTAD

Scan Direction	J_{SC} [mA/cm^2]	V_{OC} [V]	FF	PCE [%]	R_s [Ωcm^2]	R_{sh} [Ωcm^2]
Forward	21.0	0.96	0.68	13.6	4.6	2.7×10^3
Reverse	20.9	0.96	0.71	14.2	5.2	3.7×10^4

Components in the solution for the deposition of hole-transporting layer: Spiro-OMeTAD (0.050 M), FK209 (0.005 M), TBP (0.165 M), and LiTFSI (0.027 M) in chlorobenzene.

Table S4. Summary of Photovoltaic Parameters Derived from *J–V* Measurements of Perovskite Solar Cells using 2–4

HTM	Co(III) Dopant [eq.]	J_{SC} [mA/cm^2]	V_{OC} [V]	FF	PCE [%]	R_s [Ωcm^2]	R_{sh} [Ωcm^2]
2	0.0	14.1	0.84	0.36	4.3	34	1.3×10^2
2	0.15	15.9	0.91	0.67	9.7	4.7	8.2×10^2
3	0.0	17.3	0.91	0.54	8.5	8.5	2.7×10^2
3	0.15	17.1	0.87	0.53	7.9	5.2	4.1×10^2
4	0.0	1.20	0.78	0.35	0.32	350	9.6×10^2
4	0.15	2.31	0.70	0.28	0.45	180	3.4×10^2

Components in the solution for the deposition of hole-transporting layer: HTM (0.050 M), FK209 (0.0 or 0.0075 M), TBP (0.165 M), and LITFSI (0.027 M) in chlorobenzene.

As shown in Figure S14–S19, the cross-sectional SEM images demonstrate that the film morphology for all doped HTM layers is comparable, suggesting that the observed difference of photovoltaic performance between the cells using these materials does not depend on the morphology of the films.

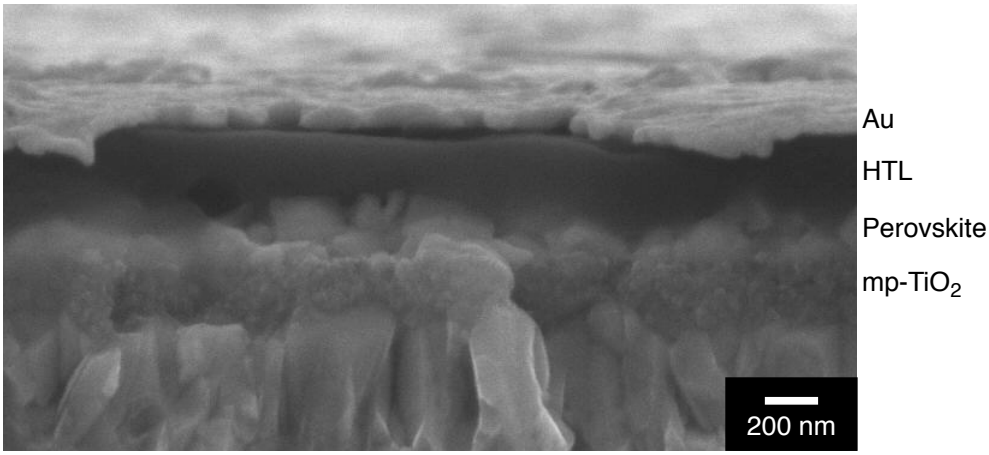

Figure S14. Cross-sectional SEM image for perovskite solar cell using **1** with 0.15 eq. Co (III) dopant, in which perovskite layer was fabricated by two-step solution method.

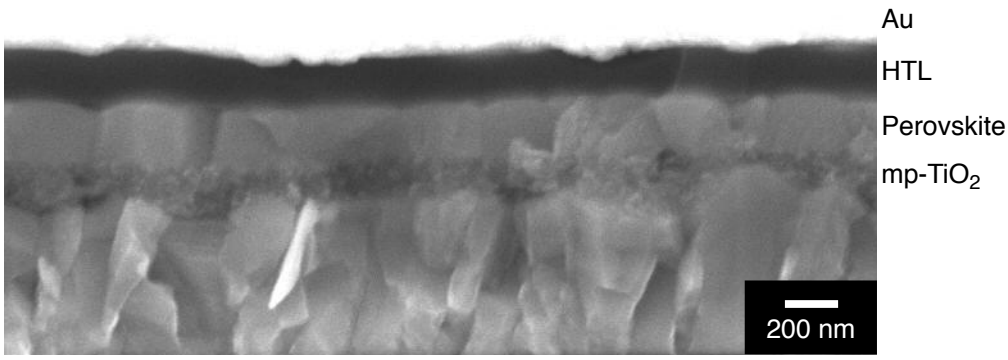

Figure S15. Cross-sectional SEM image for perovskite solar cell using **1** with 0.15 eq. Co (III) dopant, in which perovskite layer was fabricated by one-step solution method.

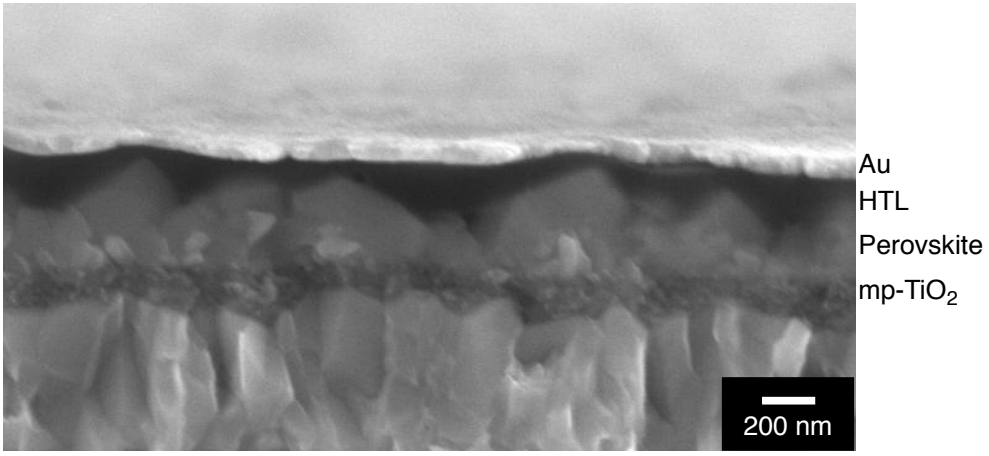

Figure S16. Cross-sectional SEM image for perovskite solar cell using **2** with 0.15 eq. Co (III) dopant, in which perovskite layer was fabricated by two-step solution method.

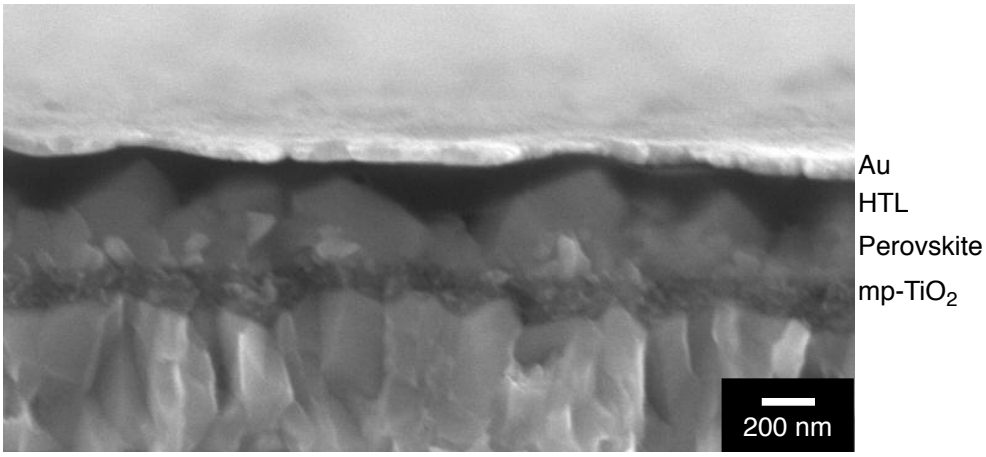

Figure S17. Cross-sectional SEM image for perovskite solar cell using **3** with 0.15 eq. Co (III) dopant, in which perovskite layer was fabricated by two-step solution method.

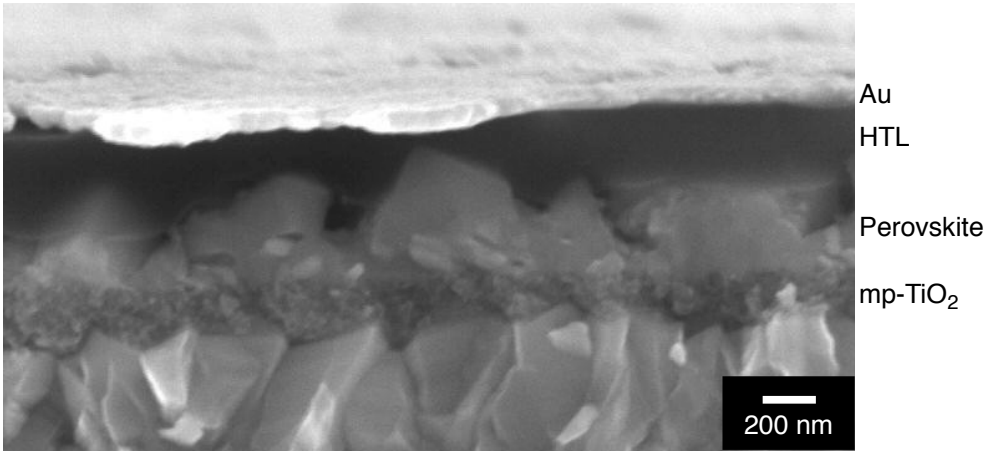

Figure S18. Cross-sectional SEM image for perovskite solar cell using **4** with 0.15 eq. Co (III) dopant, in which perovskite layer was fabricated by two-step solution method.

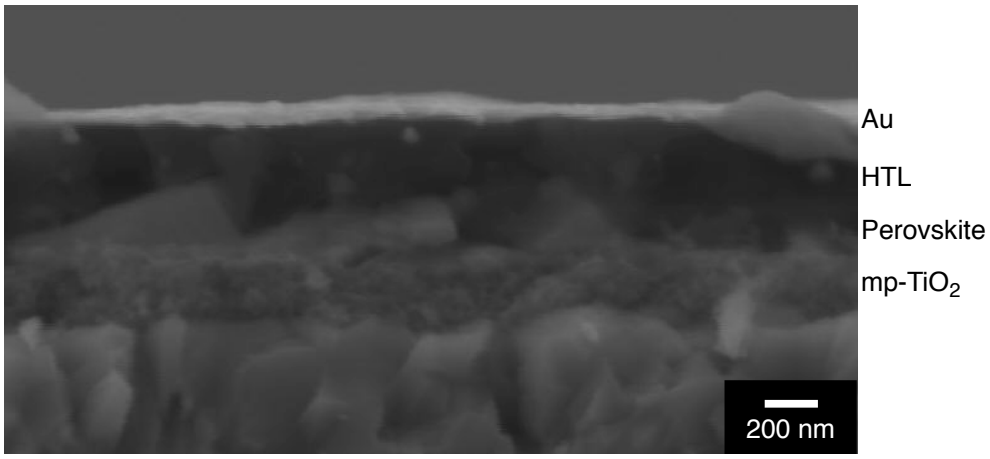

Figure S19. Cross-sectional SEM image for perovskite solar cell using Spiro-OMeTAD with 0.10 eq. Co (III) dopant, in which perovskite layer was fabricated by two-step solution method.

Space-charge-limitation of current (SCLC) method.[7]

The hole mobilities in the films of materials were measured from the space-charge-limitation of current (SCLC) *J–V* characteristics obtained in the dark for hole-only devices. Hole mobilities were calculated using the Mott-Gurney law by fitting Equation 1, where J is the current density, ε_0 is the permittivity of free space (8.85×10^{-12} F/m), ε is the relative permittivity of the material (approaching 3 for organic semiconductors), μ is the hole mobility, V is the applied voltage, and d is the thickness of the active layer, respectively.

$$J = \frac{9}{8} \varepsilon\varepsilon_0 \mu \frac{V^2}{d^3} \qquad 1$$

The ITO-coated glass substrate (5 Ω/sq, 2.5 cm × 2.5 cm, GEOMATEC) was washed carefully under ultrasonic irradiation using acetone (15 min), and ethanol (15 min). The substrate was further cleaned with a Filgen UV230 UV/ozone cleaner. A thin layer of PEDOT:PSS (Nagase ChemteX, Denatron PT-100) was prepared onto the ITO surface by the spin-coating (5000 rpm, 60 s). The resulting substrate was heated at 200 °C for 10 min under ambient conditions. Then, hole transporting layer was prepared onto PEDOT:PSS layer by spin-coating (slope 5 s, 2000 rpm, 40 s, slope 5 s) of chlorobenzene solution of hole transporting material with a concentration of 60 mmol/L. The film thicknesses were measured with Alpha-Step IQ (KLA-Tencor Co.). As a counter electrode, Au was deposited on the film by vacuum evaporation. The current density–voltage curves of the devices were taken with a Keithley 2400 source.

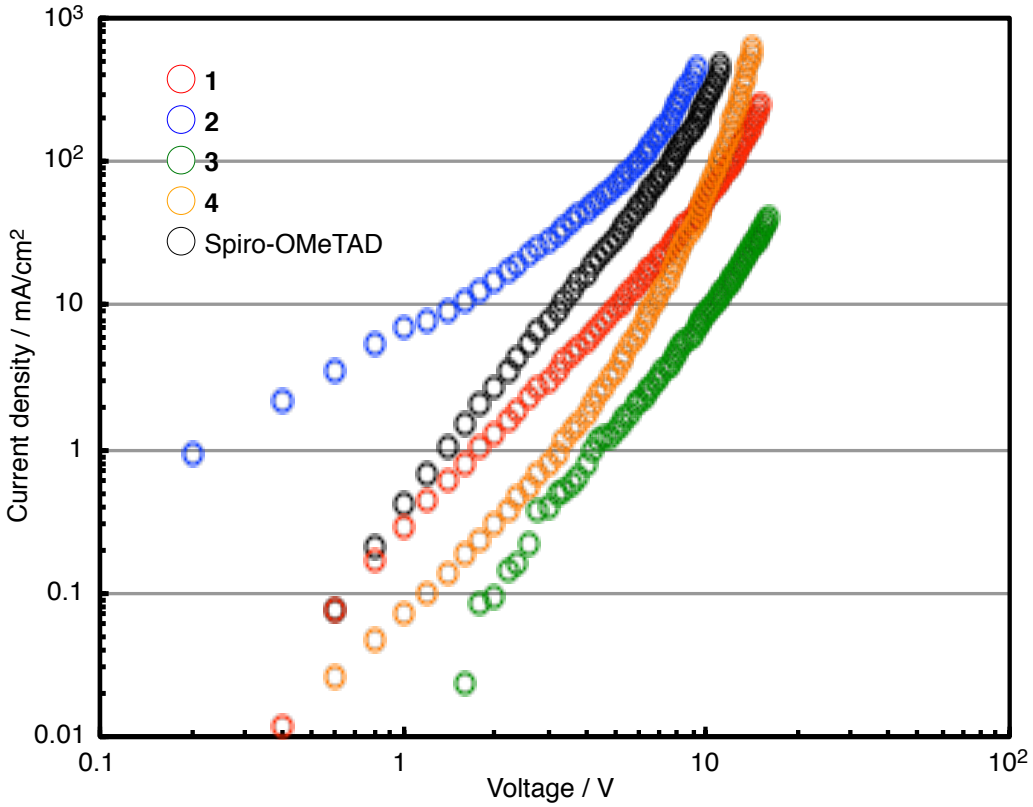

Figure S20. *J–V* characteristics of space-charge-limited current of non-doped HTMs. Relatively low threshold voltages indicate that these SCLC devices have ohmic contact.

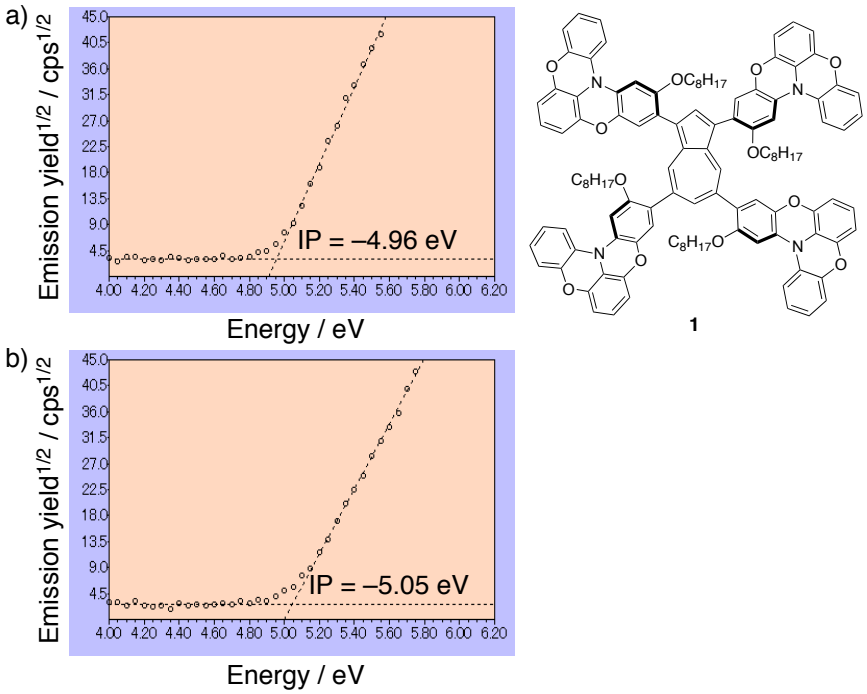

Figure S21. Photoelectron spectra measured for the spin-coated film of a) **1** and b) **1** with Co(III) dopant (0.15 eq.).

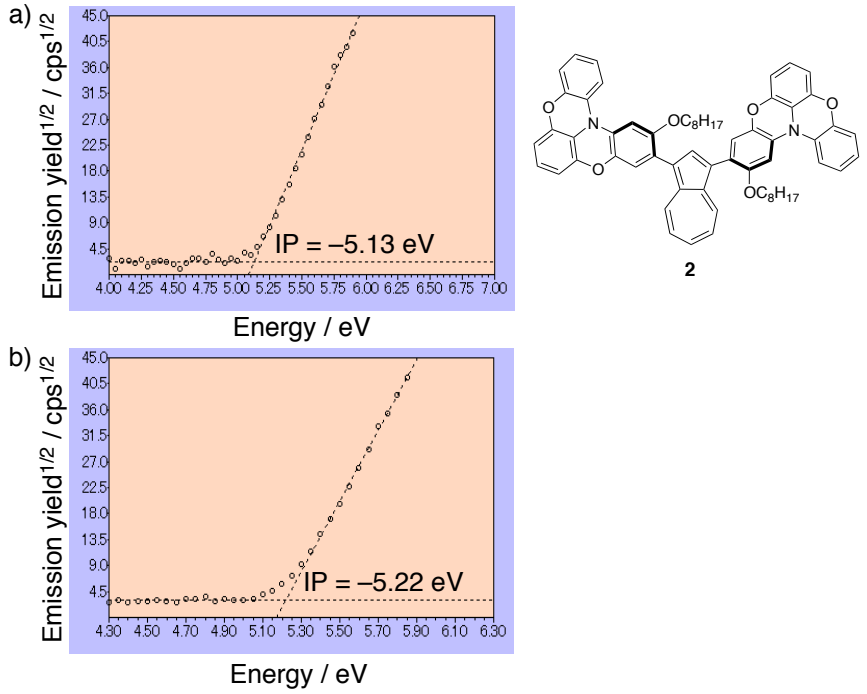

Figure S22. Photoelectron spectra measured with the spin-coated film of a) **2** and b) **2** with Co(III) dopant (0.15 eq.).

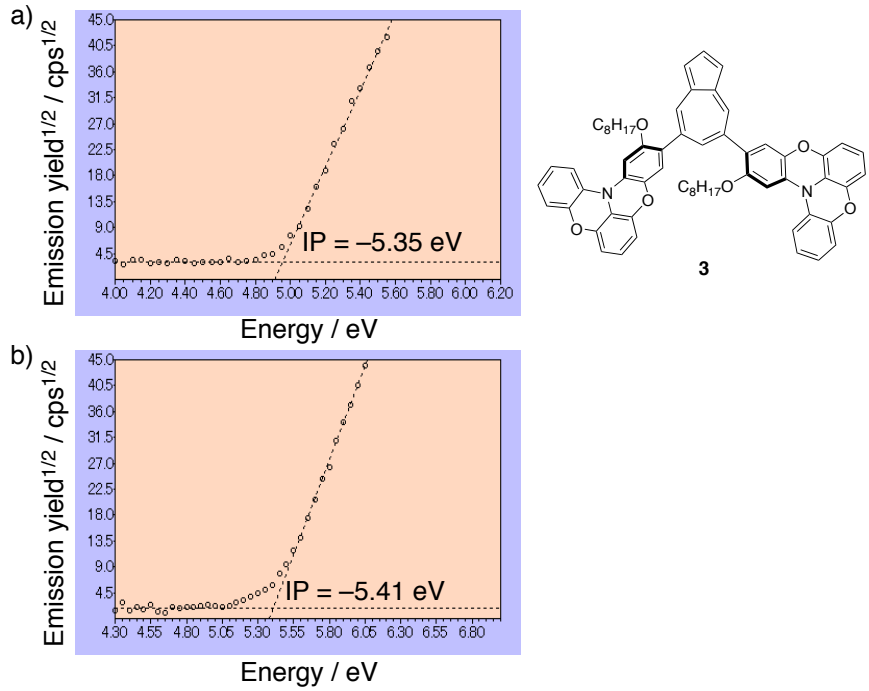

Figure S23. Photoelectron spectra measured for the spin-coated film of a) **3** and b) **3** with Co(III) dopant (0.15 eq.).

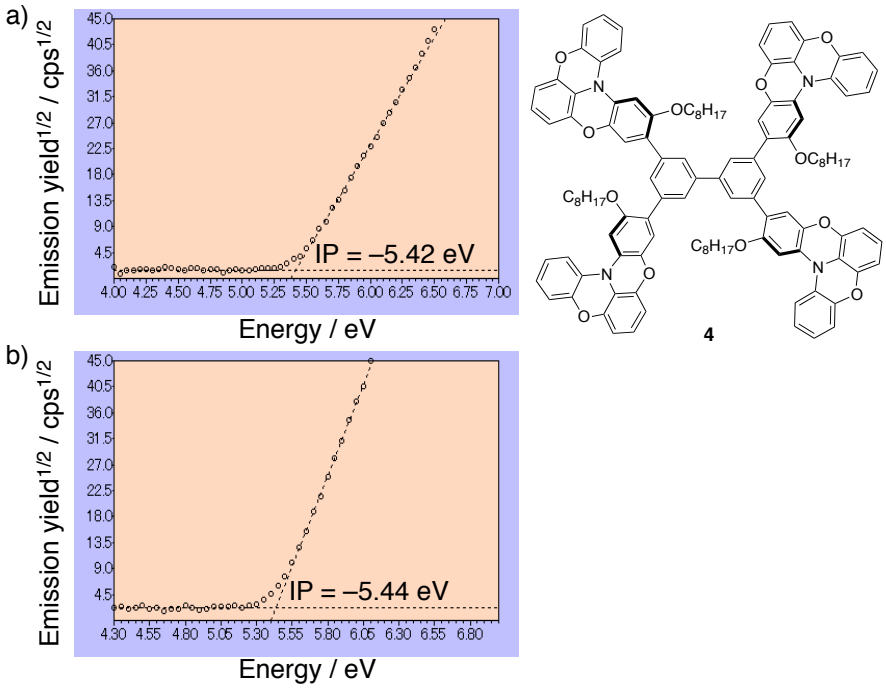

Figure S24. Photoelectron spectra measured for the spin-coated film of a) **4** and b) **4** with Co(III) dopant (0.15 eq.).

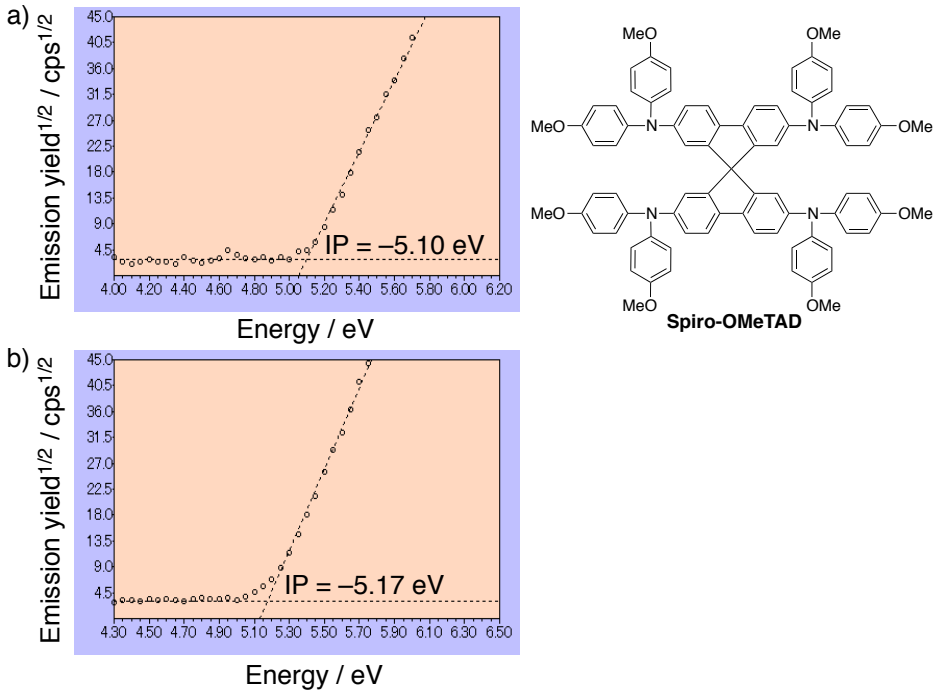

Figure S25. Photoelectron spectra measured for the spin-coated film of a) Spiro-OMeTAD and b) Spiro-OMeTAD with Co(III) dopant (0.10 eq.).

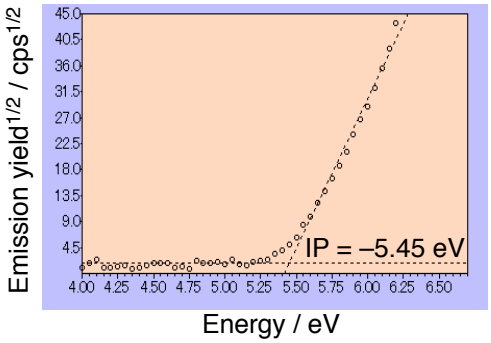

Figure S26. Photoelectron spectra measured for the perovskite ($CH_3NH_3PbI_3$) film.

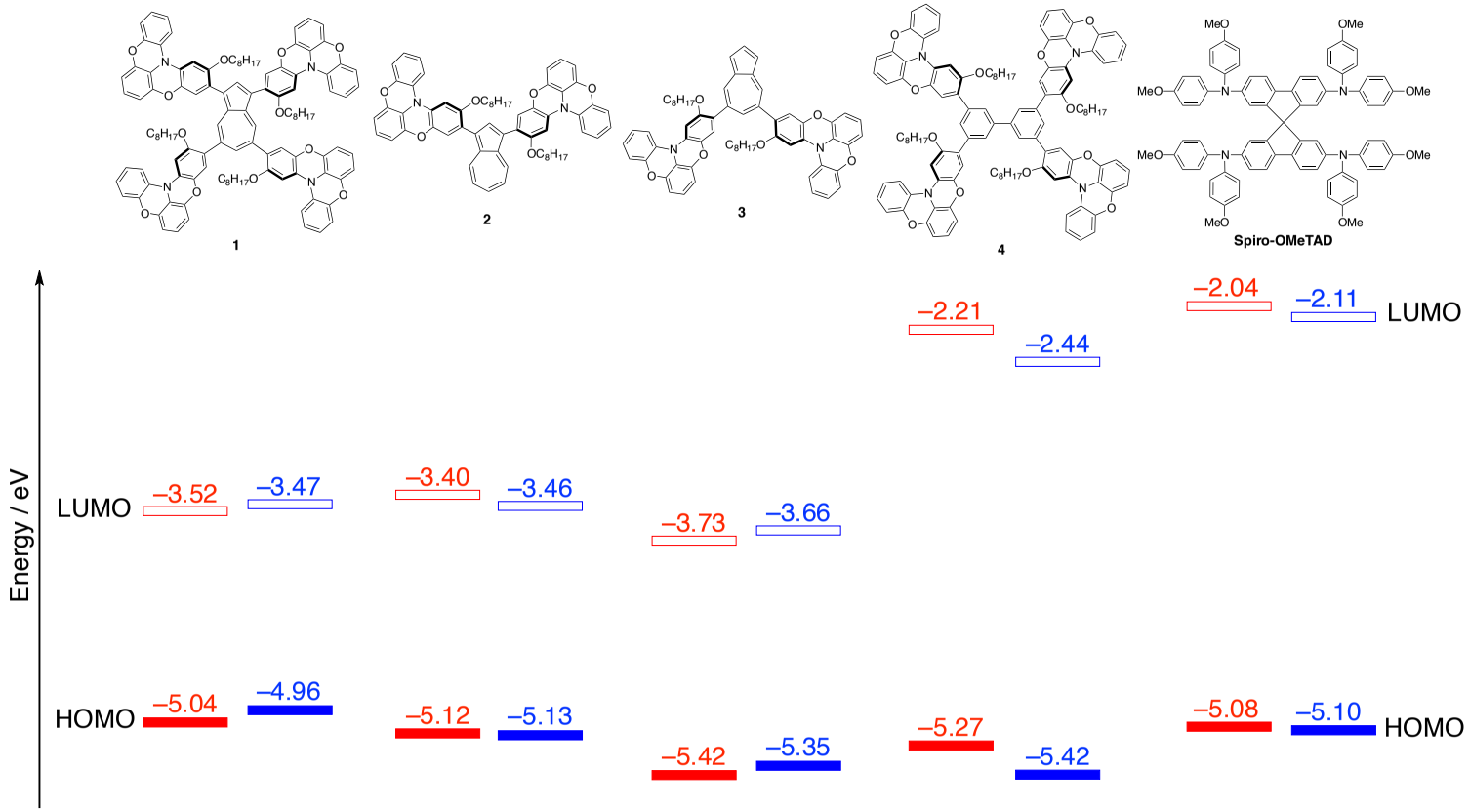

Figure S27. The HOMO and LUMO energy levels for **1–4** and Spiro-OMeTAD in CH_2Cl_2 (red) and those of spin-coated films (blue). The HOMO energy levels in solution were estimated from the onset potensials of the first oxidation peak in cyclic voltammograms (HOMO = $-(E_{1/2} + 5.1)$[8] and the LUMO energy levels were determined from the HOMO and absorption edge. The HOMO energy levels in spin-coated films were measured by photoelectron spectroscopy in air and the LUMO energy levels were determined from the HOMO and absorption edge measured for the films.

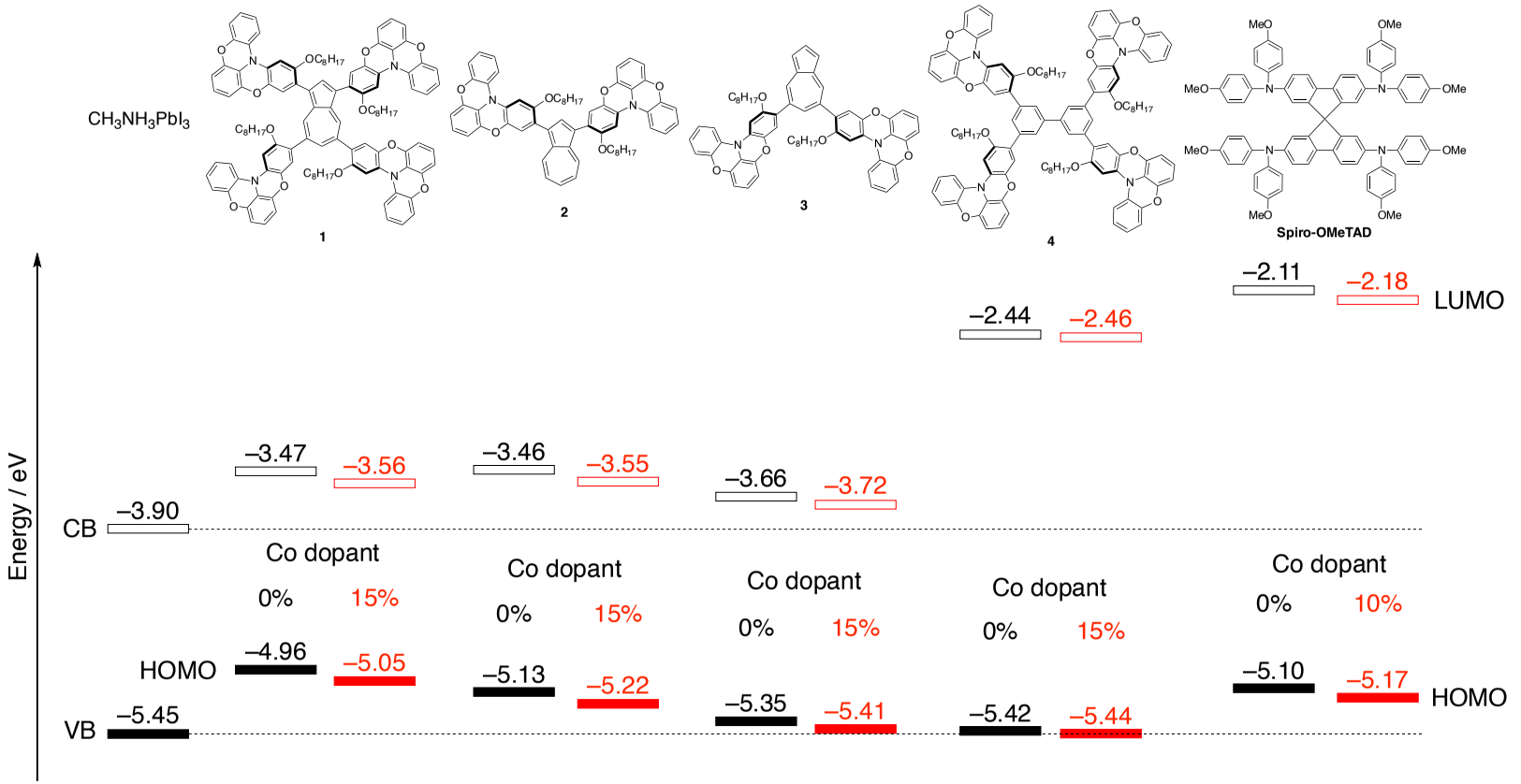

Figure S28. The HOMO and LUMO energy levels for Spiro-OMeTAD and **1–4** in neat films (black) and doped film (red). The HOMO energy levels in spin-coated films were measured by photoelectron spectroscopy in air and the LUMO energy levels were determined from the HOMO and absorption edge measured for the film.

Time-resolved microwave conductivity (TRMC) method.[9]

1) Treatment of quartz substrate

Quartz substrate (Daiko MFG Co. Ltd.) was treated with ultrasonic cleaning for 10 min with acetone and 2-propanol, respectively, and then subjected to an O_3/ultraviolet treatment for 30 min.

2) Preparation of HTM solution

A mixture of **HTM** (0.040 M) and FK209 (0–12.0 mg, 0–0.0080 M) as an oxidizing agent was dissolved in a solution containing chlorobenzene (1 mL), TBP (19.5 μL, 0.132 M, Aldrich), and LiTFSI (6.2 mg, 0.022 M, Wako Pure Chemical Industries Co., Ltd.). After 30 min, the resulting suspension was filtered with a membrane filter (Cosmonice filter S, Nacarai Tesque, Inc.) to remove the formed insoluble Co(II) complex.

3) Fabrication of HTM sample

In a glove box filled with an inert gas, the hole-transporting layer was deposited on the quartz substrate by spin-coating (slope 5 s, 2000 rpm, 40 s, slope 5 s) of the solution of each **HTM**. The resulting film was dried on a hot plate (at 40 °C for **1–4** and at 70 °C for Spiro-OMeTAD, respectively) for 30 min.

4) Fabrication of perovskite (mesoporous-TiO_2/$CH_3NH_3PbI_3$) sample

Quartz substrate was covered with the mesoporous TiO_2 layer by spin-coating (slope 5 s, 5000 rpm, 30 s, slope 5 s) of a suspension of TiO_2 paste (PST–18NR, TiO_2) in ethanol (paste : ethanol = 1 : 5 wt ratio), followed by sintering at 500 °C for 20 min. The obtained substrate was treated with ultraviolet-ozone cleaning for 15 min before used for perovskite layer fabrication. In a glove box filled with an inert gas, a 0.75 M solution of PbI_2 in dehydrated DMF (70 °C) was deposited on the mesoporous TiO_2 films by spin-coating (slope 5 s, 4000 rpm, 20 s, slope 5 s). The resulting yellow film was annealed on a hot plate at 70 °C for 1 h. The film was dipped for 40 s in a 0.06 M solution of CH_3NH_3I in 2-propanol. The formed

perovskite film was then annealed on a hot plate at 70 °C for 1 h. The hole-transporting layer was deposited on the perovskite layer by spin-coating (slope 5 s, 2000 rpm, 40 s, slope 5 s) of the solution of **HTM**. The resulting film was dried on a hot plate (at 40 °C for **1–4** and at 70 °C for Spiro-OMeTAD, respectively) for 30 min.

5) TRMC measurement

Transient photoconductivity was measured by flash-photolysis time-resolved microwave conductivity (FP-TRMC). A resonant cavity was used to obtain a high degree of sensitivity in the measurement of conductivity. The resonant frequency was set at ~9.1 GHz and the microwave power was set at 3 mW, so that the electric field of the microwave was sufficiently small not to disturb the motion of charge carriers. The value of conductivity is converted to the product of the quantum yield ϕ and the sum of charge carrier mobilities $\Sigma\mu$, by $\phi\Sigma\mu = \Delta\sigma (eI_0F_{\text{light}})^{-1}$, where e, I_0, F_{light}, and $\Delta\sigma$ are the unit charge of a single electron, incident photon density of excitation laser (photons/m^2), a correction (or filling) factor (/m), and a transient photoconductivity, respectively. The change of conductivity is equivalent with $\Delta P_r/(AP_r)$, where ΔP_r, P_r, and A are change of reflected microwave power, a power of reflected microwave, and a sensitivity factor [(S/m)$^{-1}$], respectively. Third harmonic generation (355 nm for HTM-only samples and 550 nm for perovskite samples w/wo HTL) from an Optical Parametric Oscillator (OPO) of a Nd:YAG laser (Continuum Surelite II, 5–8 ns pulse duration) was used as an excitation source. The incident photon density of HTM-only sample and perovskite sample were set at 4.6×10^{15} photons/cm^2 and 1.4×10^{11} photons/cm^2, respectively. The sample was set at the highest electric field in a resonant cavity. FP-TRMC experiments were performed at room temperature.

The values of ϕ in the compounds were determined by conventional photo-current measurement[9b] in a vacuum chamber (10^{-4} Pa) using an inter-digitated Au electrodes on a glass substrate with 5 μm gap under excitation at 355 nm with the photon density of 4.6×10^{15} photons/cm^2. Transient current was predominantly observed on the film sample under the applied bias of 0–10 V (0–2.0×10^4 Vcm^{-1}), and monitored by a Tektronix TDS3032B digital oscilloscope.

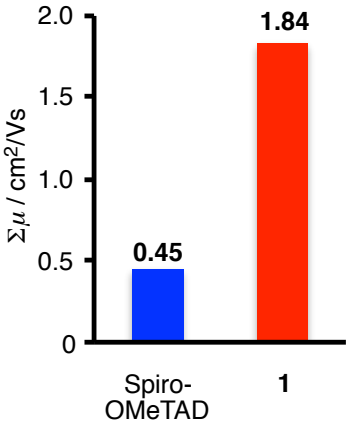

Figure S29. Local mobility ($\Sigma\mu$) in non-doped films of Spiro-OMeTAD (blue) and **1** (red) measured by TRMC.

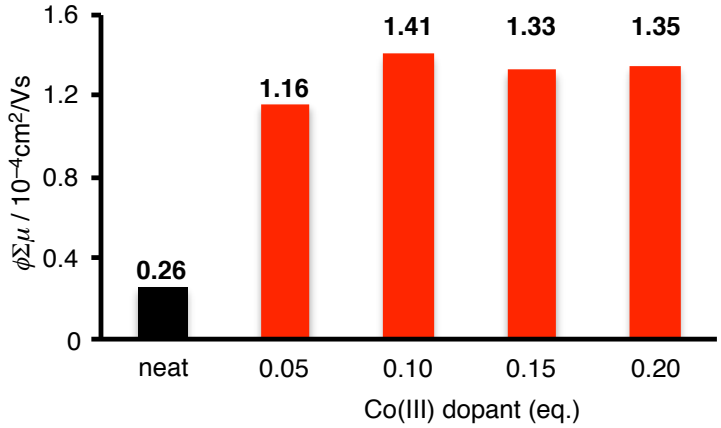

Figure S30. Maximum TRMC signal ($\phi\Sigma\mu$) for the spin-coated neat film (black) and Co(III) doped films (red) of **1**. The films were prepared by deposition of the solution containing additives, LiTFSI (0.54 eq.), TBP (3.3 eq.) and Co(III) dopant (0.0–0.15 eq.).

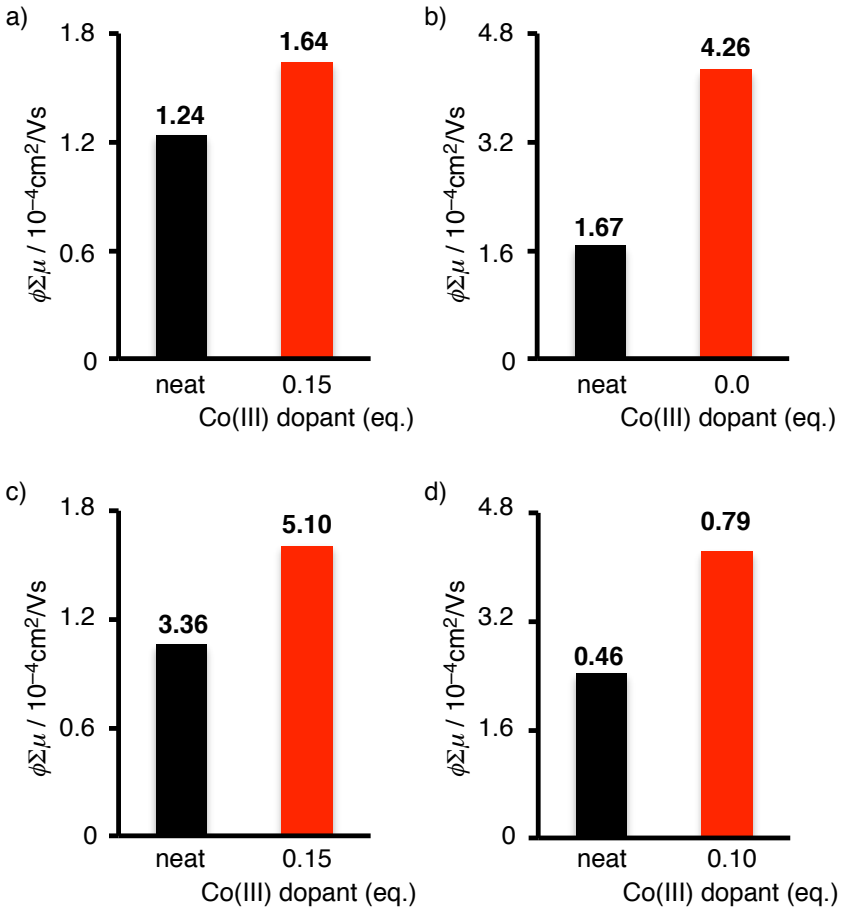

Figure S31. Maximum TRMC signal ($\phi\Sigma\mu$) for the spin-coated film (neat (black) and doped (red) HTMs): (a) **2**, (b) **3**, (c) **4**, (d) Spiro-OMeTAD. The films were prepared by deposition of the solution containing additives, LiTFSI (0.54 eq.), TBP (3.3 eq.) and Co(III) dopant (0.0–0.15 eq.).

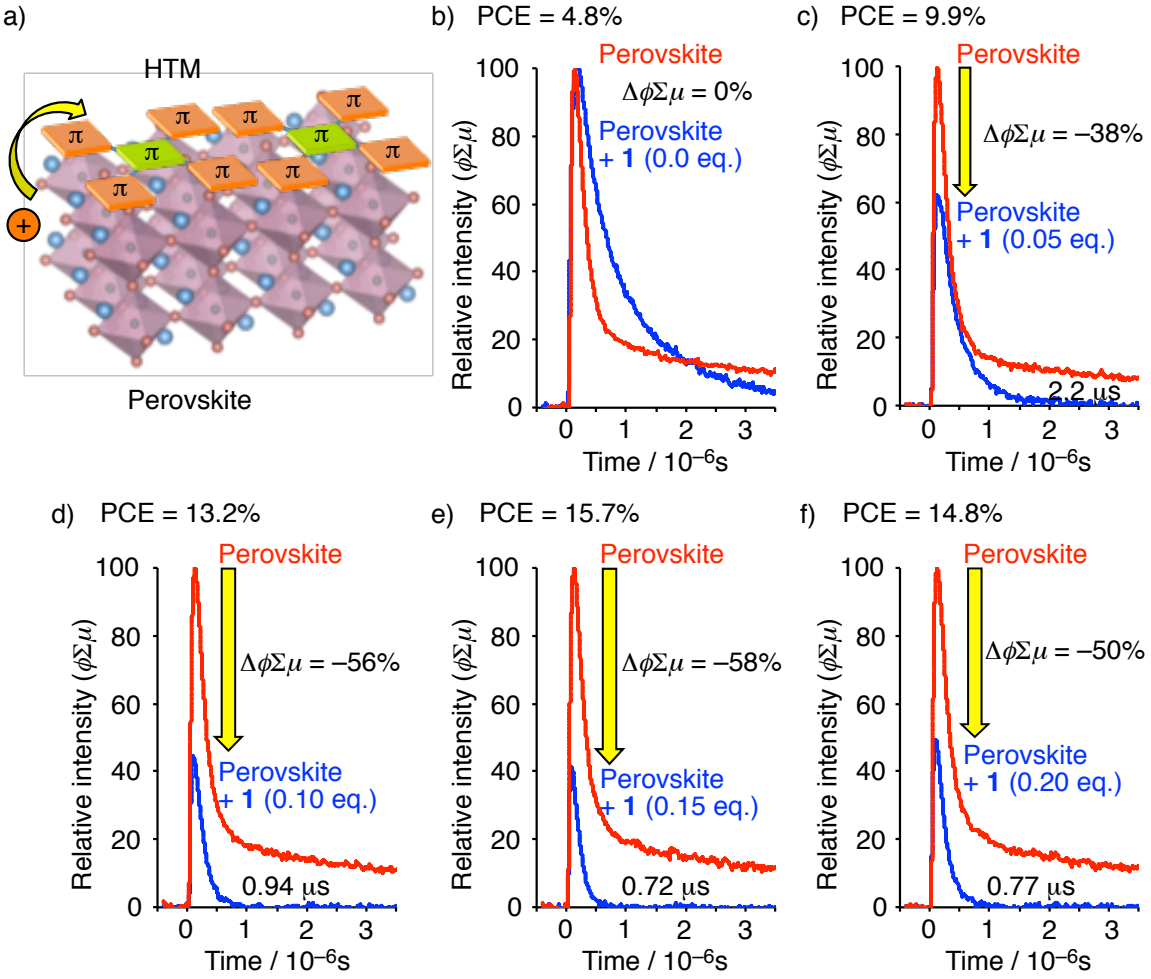

Figure S32. a) Image of charge collection at the interface between perovskite and hole-transporting layer. b–f) $\phi\Sigma\mu$ transients of perovskite films prior (red) posterior (blue) to **1** coating at a photon flux of $I_0 = 1.4 \times 10^{11}$ photons/cm^2 with different amount of Co(III) dopant ((b) 0.0 eq., (c) 0.05 eq., (d) 0.10 eq., (e) 0.15 eq., and (f) 0.20 eq.).

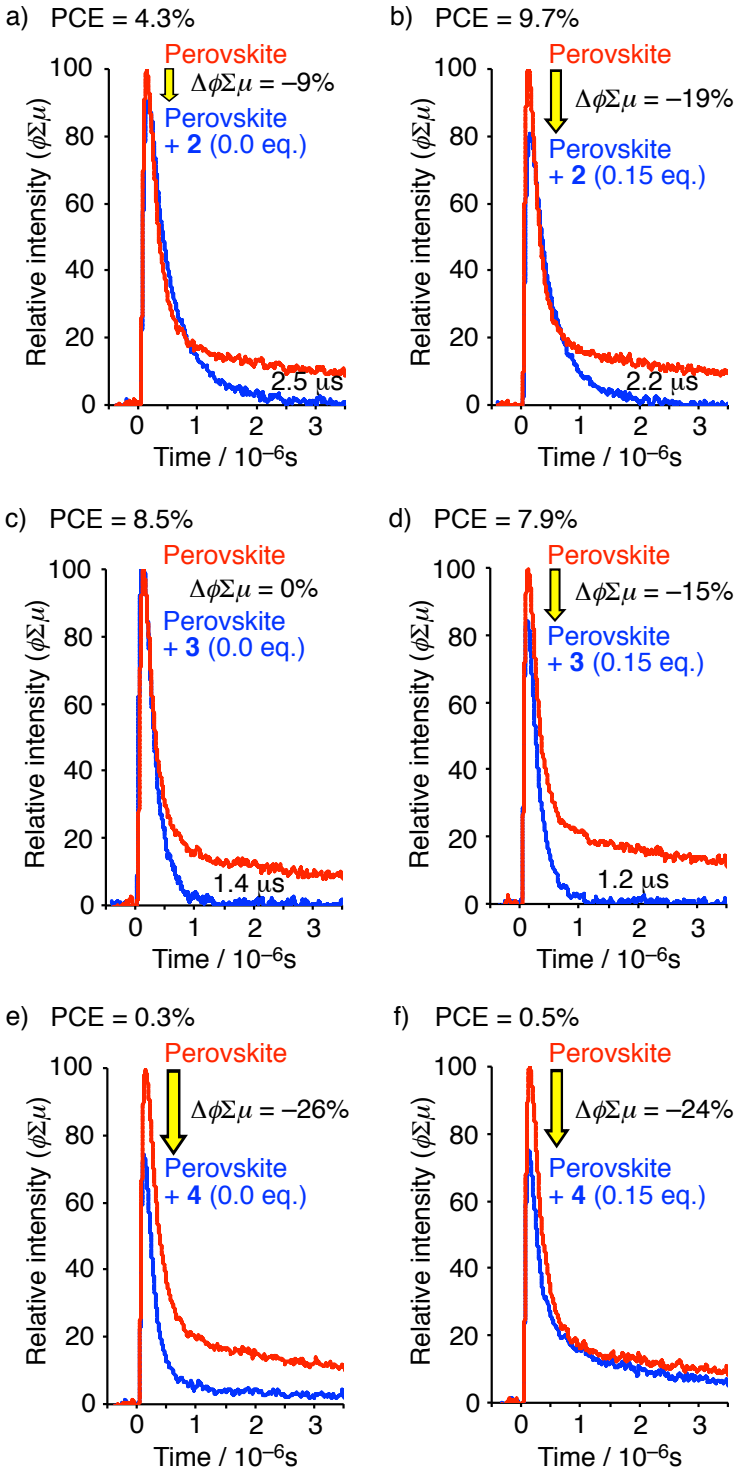

Figure S33. $\phi\Sigma\mu$ transients of perovskite films prior (red) posterior (blue) to HTM coating at a photon flux of $I_0 = 1.4 \times 10^{11}$ photons/cm^2: (a) **2** (Co(III): 0.0 eq.), (b) **2** (0.15 eq.), (c) **3** (0.0 eq.), (d) **3** (0.15 eq.), (e) **4** (0.0 eq.), and (f) **4** (0.15 eq.).

A good correlation was observed between the PCEs of the solar cells and the extent of transient decay in TRMC measurements for **1–4** as well as the effects of the amount of Co(III) dopant for **1**.

Table S5. Summary for the Parameters in Perovskite Solar Cells and the Transient Decay of TRMC Measurements for 1–4

HTM	Co(III) Dopant [eq.]	J_{SC} [mA/cm^2]	V_{OC} [V]	FF	PCE [%]	R_s [Ωcm^2]	R_{sh} [Ωcm^2]	$\Delta\phi\Sigma\mu$ [%]	time [μs]
1	0.0	14.9	0.82	0.39	**4.8**	15	1.2×10^2	**0**	–
1	0.05	18.2	0.96	0.57	**9.9**	6.8	2.1×10^2	**–38**	**2.2**
1	0.10	20.1	0.99	0.66	**13.2**	7.0	7.4×10^2	**–56**	**0.94**
1	0.15	20.7	1.04	0.73	**15.7**	8.6	1.6×10^3	**–58**	**0.72**
1	0.20	20.5	1.02	0.71	**14.8**	6.8	1.6×10^3	**–50**	**0.77**
2	0.0	14.1	0.84	0.36	**4.3**	34	1.3×10^2	**–9**	**2.5**
2	0.15	15.9	0.91	0.67	**9.7**	4.7	8.2×10^2	**–19**	**2.2**
3	0.0	17.3	0.91	0.54	**8.5**	8.5	2.7×10^2	**0**	**1.4**
3	0.15	17.1	0.87	0.53	**7.9**	5.2	4.1×10^2	**–15**	**1.2**
4	0.0	1.20	0.78	0.35	**0.32**	350	9.6×10^2	**–26**	–
4	0.15	2.31	0.70	0.28	**0.45**	180	3.4×10^2	**–24**	–

References

1. Gaussian 09 (Revision A.02), M. J. Frisch, G. W. Trucks, H. B. Schlegel, G. E. Scuseria, M. A. Robb, J. R. Cheeseman, G. Scalmani, V. Barone, B. Mennucci, G. A. Petersson, H. Nakatsuji, M. Caricato, X. Li, H. P. Hratchian, A. F. Izmaylov, J. Bloino, G. Zheng, J. L. Sonnenberg, M. Hada, M. Ehara, K. Toyota, R. Fukuda, J. Hasegawa, M. Ishida, T. Nakajima, Y. Honda, O. Kitao, H. Nakai, T. Vreven, J. A. Montgomery, Jr., J. E. Peralta, F. Ogliaro, M. Bearpark, J. J. Heyd, E. Brothers, K. N. Kudin, V. N. Staroverov, R. Kobayashi, J. Normand, K. Raghavachari, A. Rendell, J. C. Burant, S. S. Iyengar, J. Tomasi, M. Cossi, N. Rega, J. M. Millam, M. Klene, J. E. Knox, J. B. Cross, V. Bakken, C. Adamo, J. Jaramillo, R. Gomperts, R. E. Stratmann, O. Yazyev, A. J. Austin, R. Cammi, C. Pomelli, J. W. Ochterski, R. L. Martin, K. Morokuma, V. G. Zakrzewski, G. A. Voth, P. Salvador, J. J. Dannenberg, S. Dapprich, A. D. Daniels, Ö. Farkas, J. B. Foresman, J. V. Ortiz, J. Cioslowski, D. J. Fox, Gaussian, Inc., Wallingford CT, 2009.
2. Wakamiya, A.; Nishimura, H.; Fukushima, T.; Suzuki, F.; Saeki, A.; Seki, S.; Osaka, I.; Sasamori, T.; Murata, M.; Murata, Y.; Kaji, H. *Angew. Chem.*, *Int. Ed.*, **2014**, *53*, 5800.
3. Nishimura, H.; Eliseeva, M. N.; Wakamiya, A.; Scott, L. T. *Synlett* **2015,** *26*, 1578.
4. Salman, H.; Abraham, Y.; Tal, S.; Meltzman, S.; Kapon, M.; Tessler, N.; Speiser, S.; Eichen, Y. *Eur. J. Org. Chem.* **2005**, 2207.
5. Eliseeva, M. N.; Scott, L. T. *J. Am. Chem. Soc.* **2012**, *134*, 15169.
6. Burschka, J.; Kessler, F.; Nazeeruddin, M. K.; Grätzel, M. *Chem. Mater.* **2013**, *25*, 2986.
7. (a) Choi, H.; Cho, J. W.; Kang, M.-S.; Ko, J. *Chem. Commun.* **2015**, *51*, 9305. (b) Steck, C.; Franckevič, M.; Zakeeruddin, S. M.; Mishra, A.; Bäuerle, P.; Grätzel, M. *J. Mater. Chem. A* **2015**, *3*, 17738.
8. Cardona, C. M.; Li, W.; Kaifer, A. E.; Stockdale, D.; Bazan, G. C. *Adv. Mater.* **2011**, *23*, 2367.
9. (a) Saeki, A.; Koizumi, Y.; Aida, T.; Seki, S. *Acc. Chem. Res.* **2012**, *45*, 1193. (b) Yasutani, Y.; Saeki, A.; Fukumatsu, T.; Koizumi, Y.; Seki, S. *Chem. Lett.* **2013**, *42*, 19. (c) Oga, H.; Saeki, A.; Ogomi, Y.; Hayase, S.; Seki, S. *J. Am. Chem. Soc.* **2014**, *136*, 13818.

^{1}H NMR (500 MHz, $CDCl_3$)

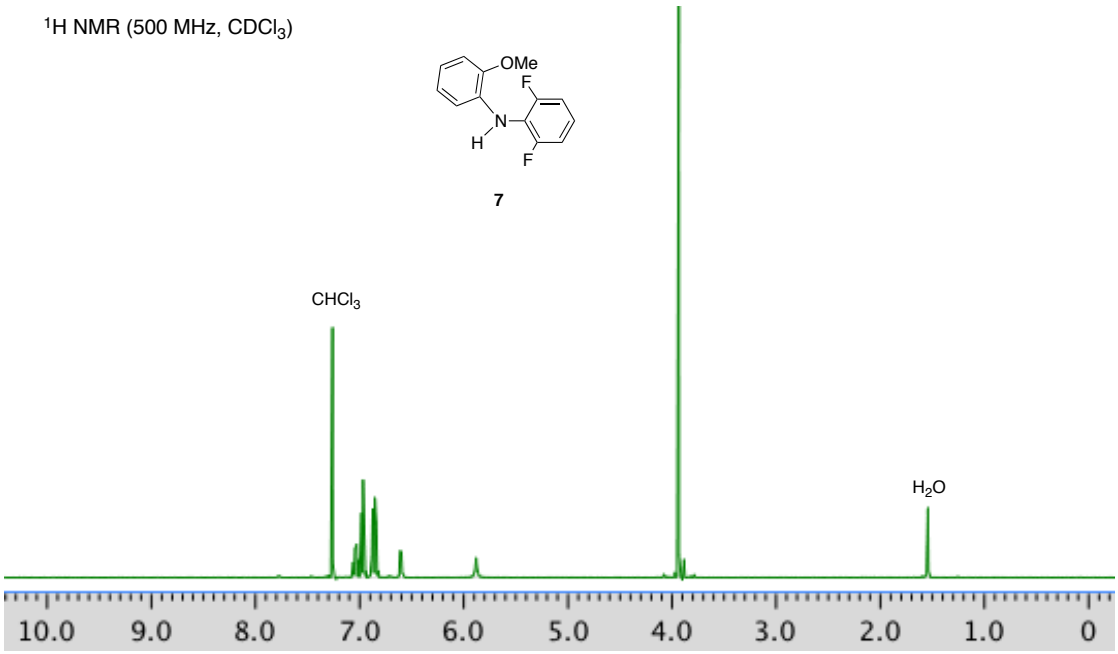

^{13}C NMR (125 MHz, $CDCl_3$)

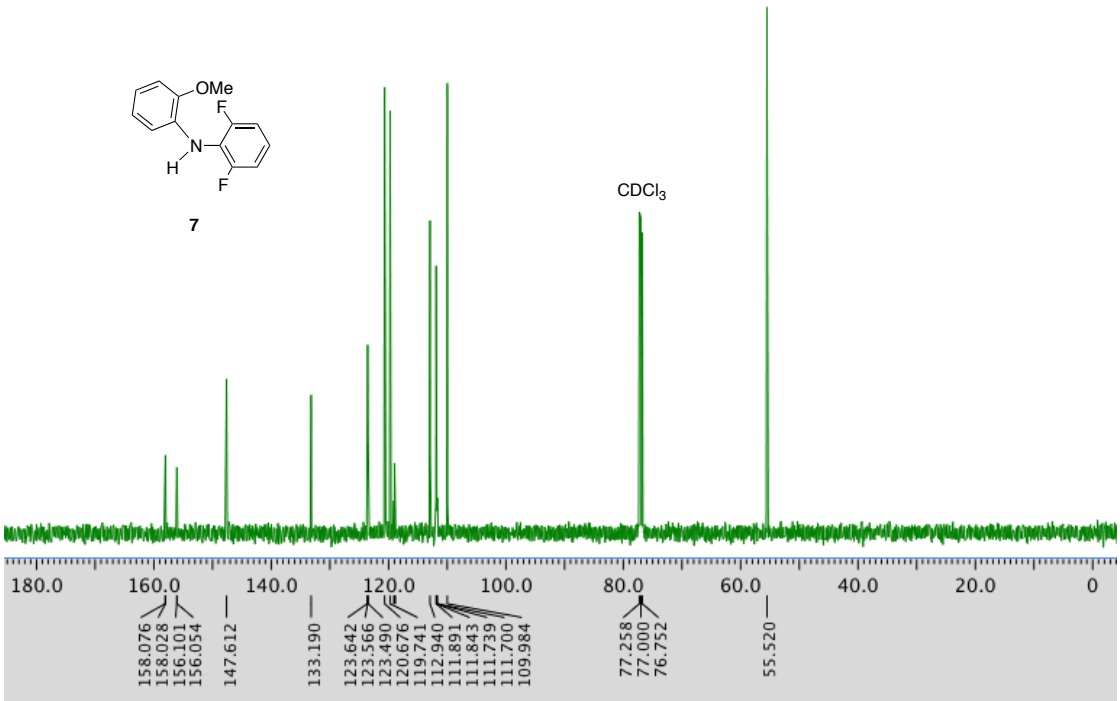

^{1}H NMR (500 MHz, $CDCl_3$)

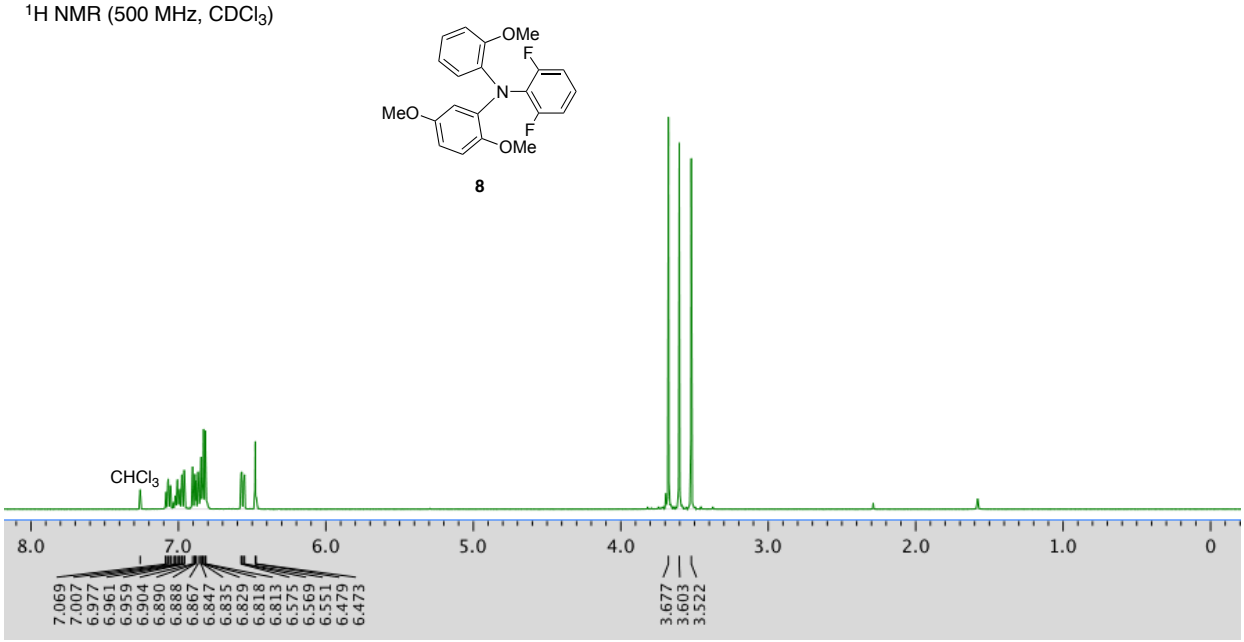

^{13}C NMR (125 MHz, $CDCl_3$)

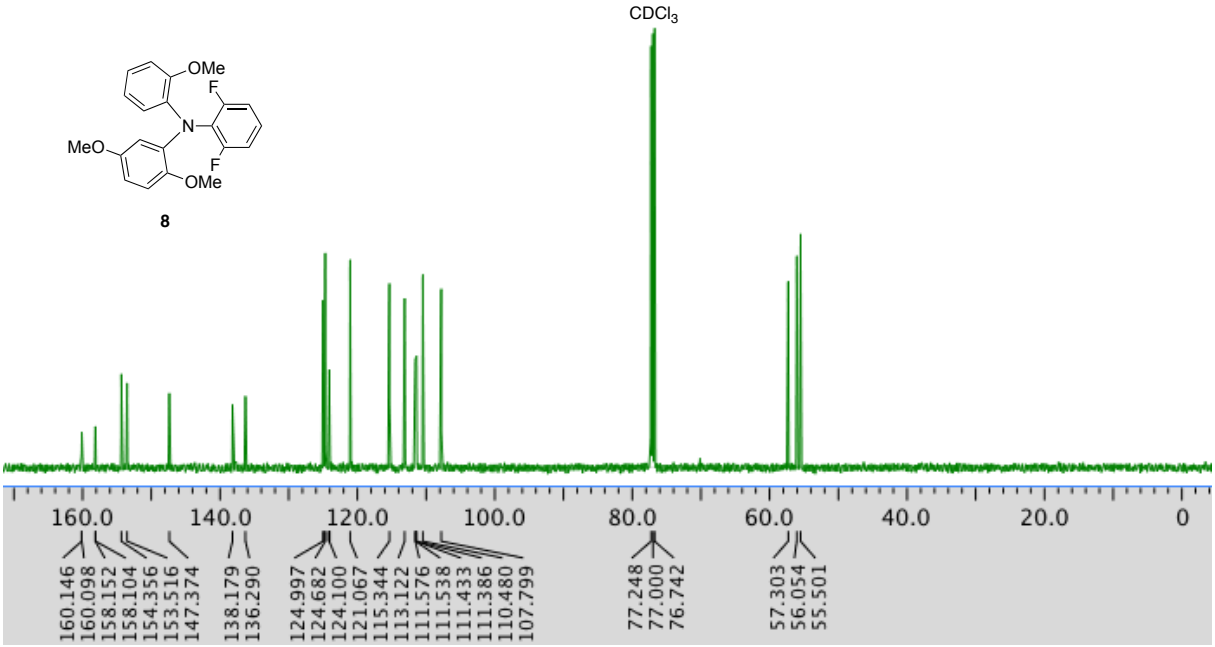

^{1}H NMR (500 MHz, CD_2Cl_2)

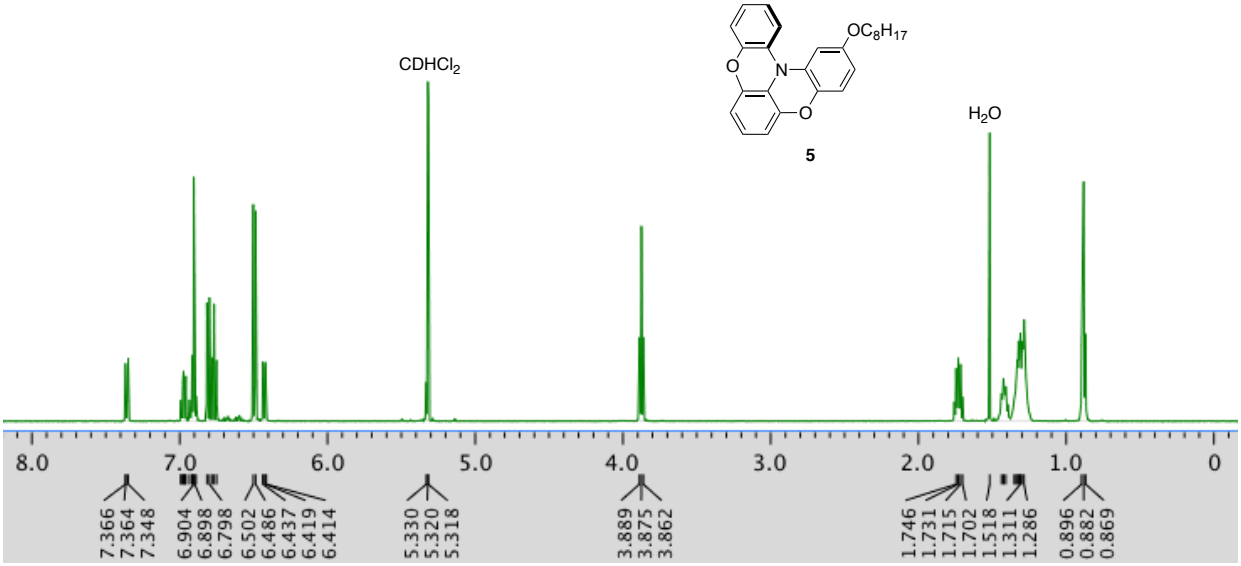

^{13}C NMR (125 MHz, CD_2Cl_2)

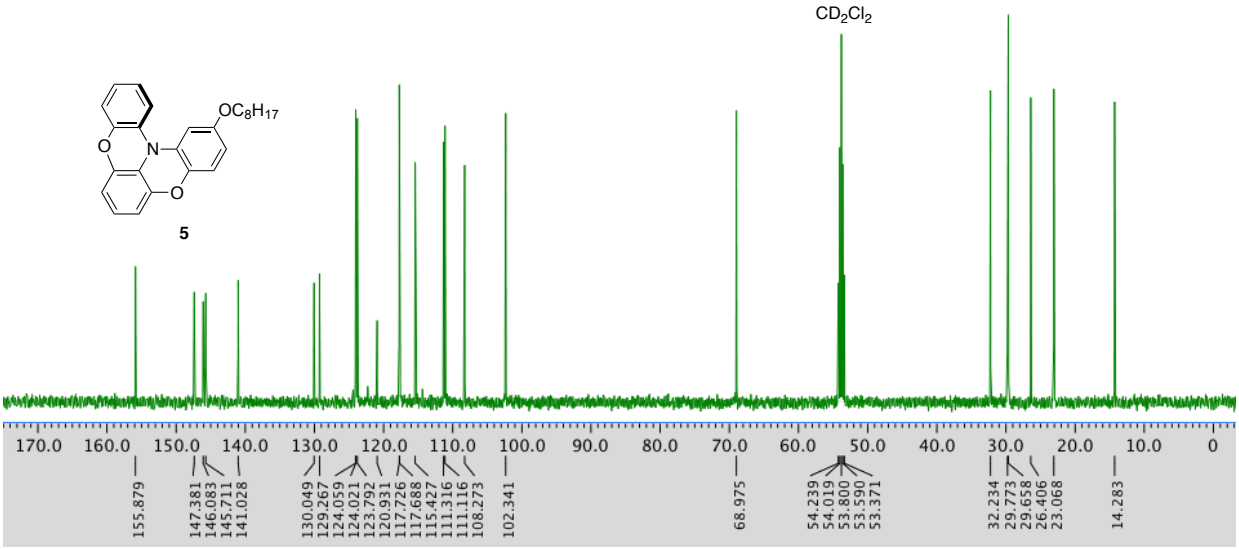

^{1}H NMR (500 MHz, CD_2Cl_2)

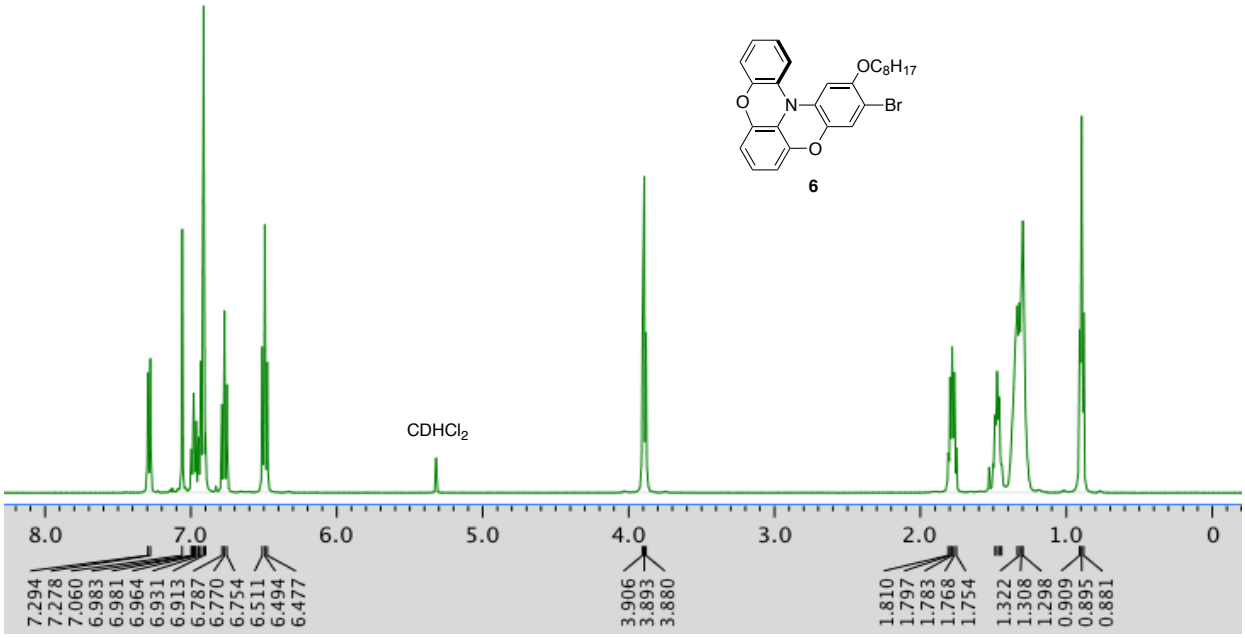

^{13}C NMR (125 MHz, CD_2Cl_2)

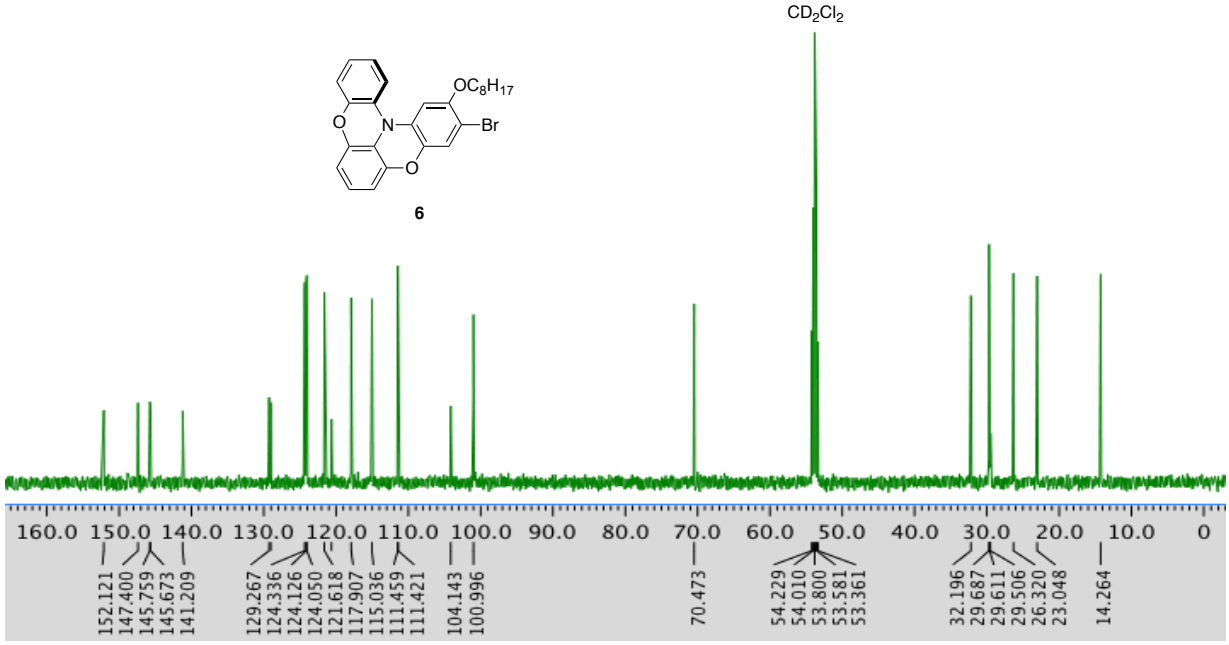

^{1}H NMR (500 MHz, CD_2Cl_2)

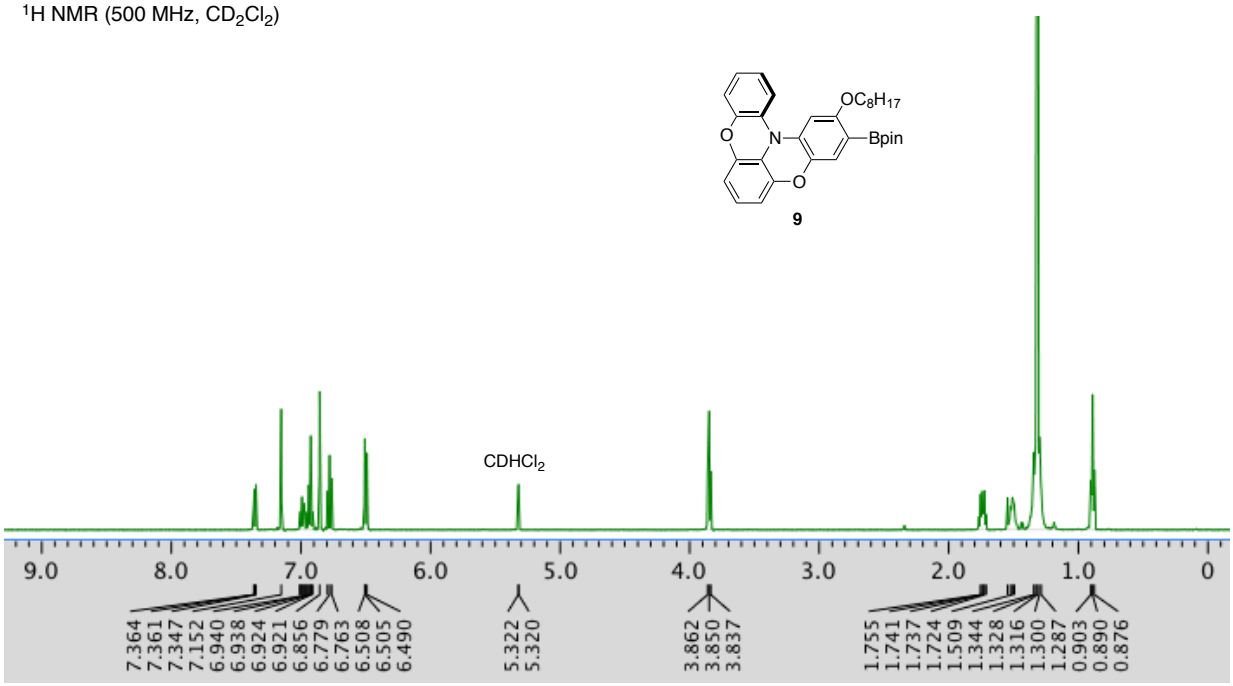

^{13}C NMR (125 MHz, CD_2Cl_2)

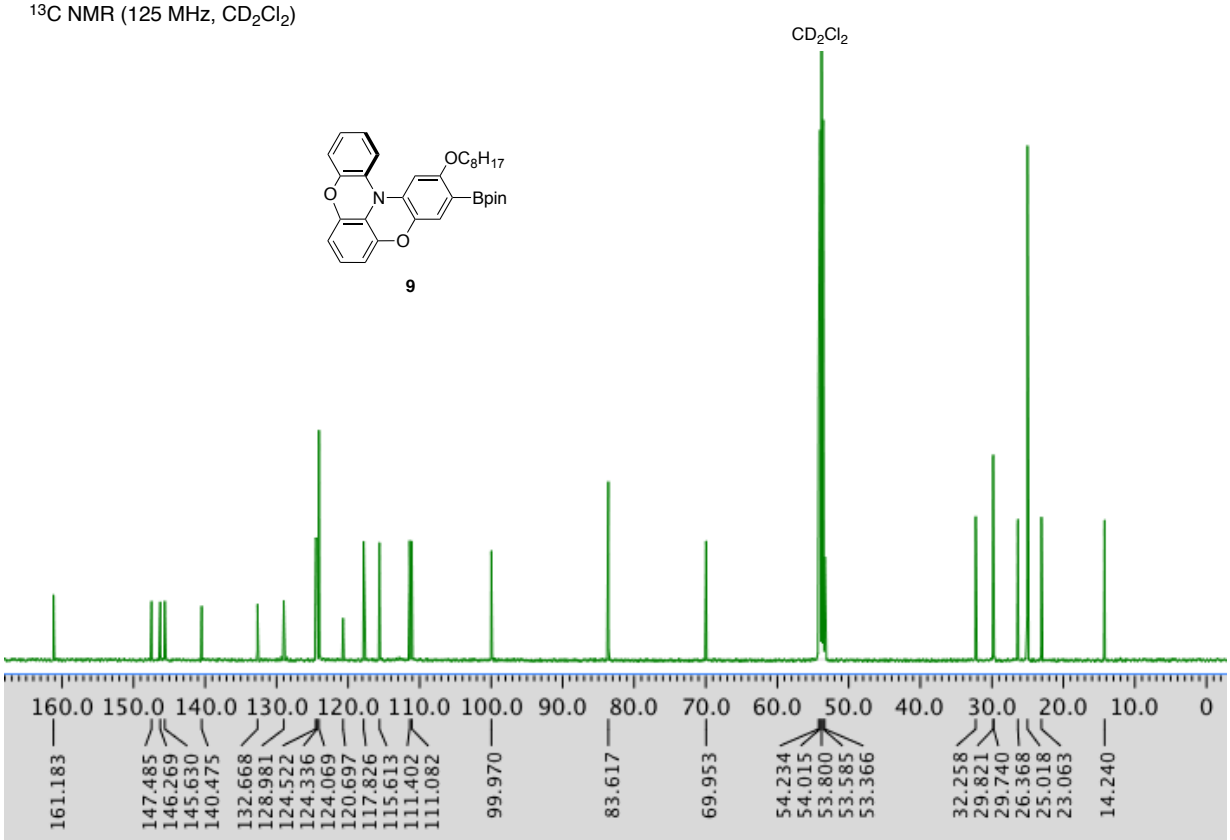

^{1}H NMR (500 MHz, CD_2Cl_2)

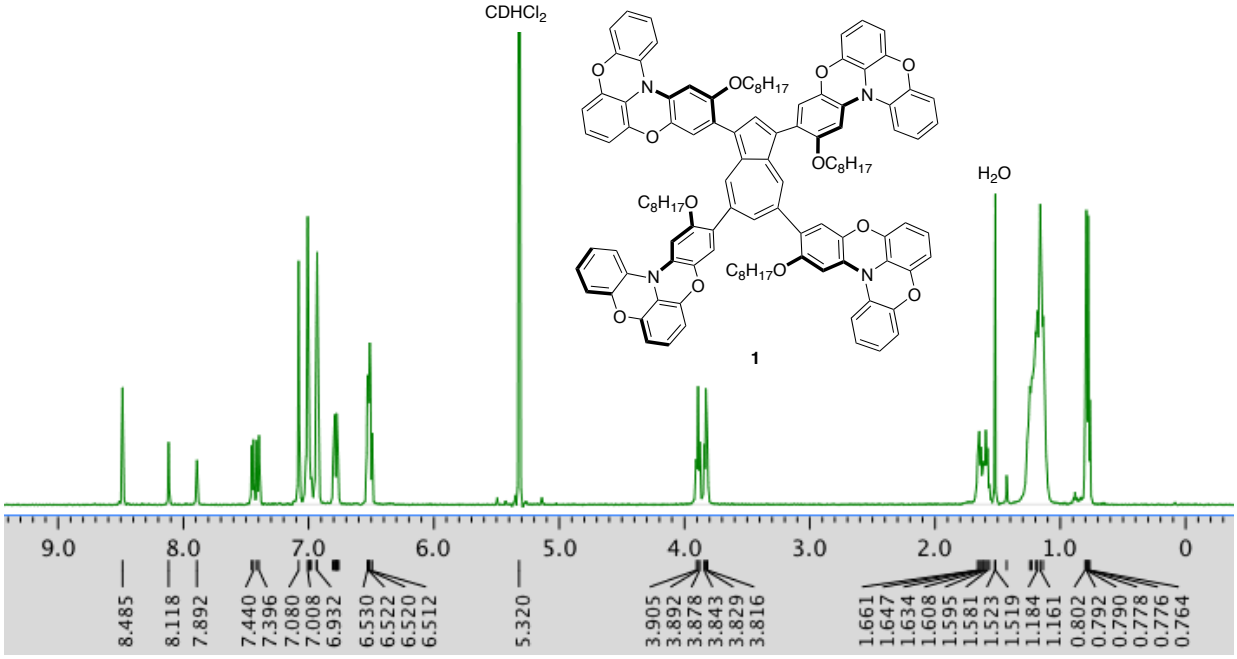

^{13}C NMR (125 MHz, CD_2Cl_2)

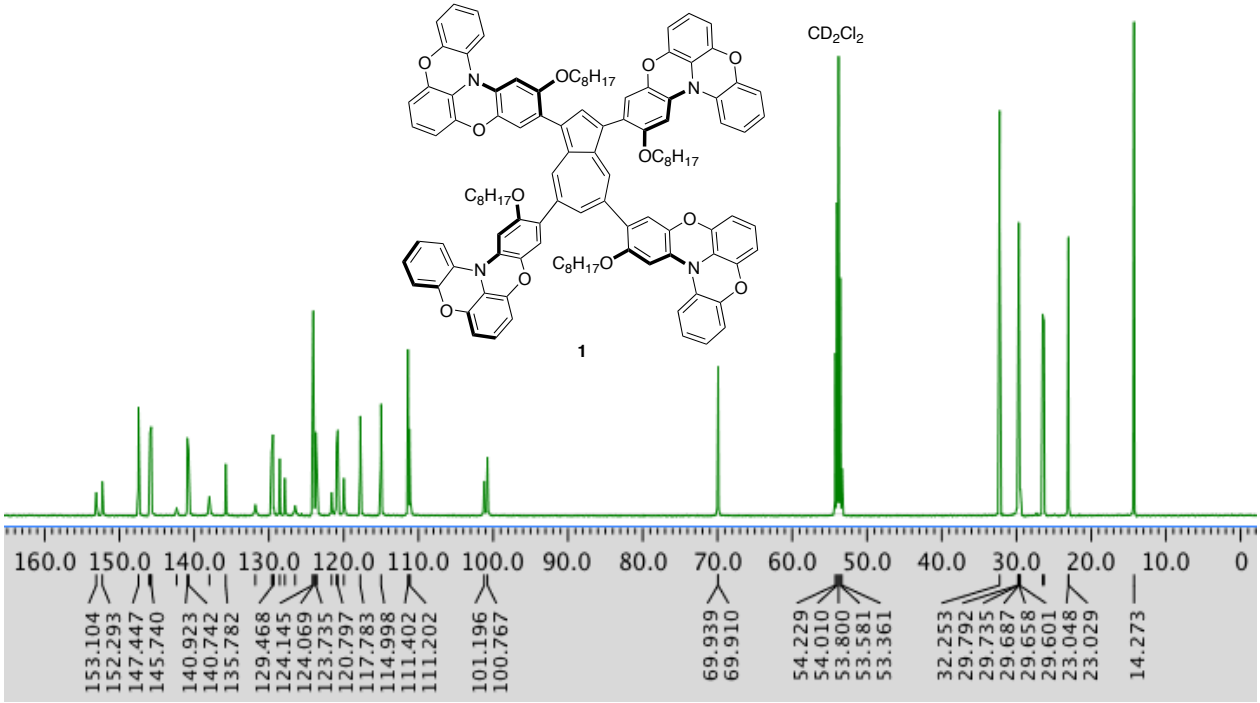

^{1}H NMR (500 MHz, CD_2Cl_2)

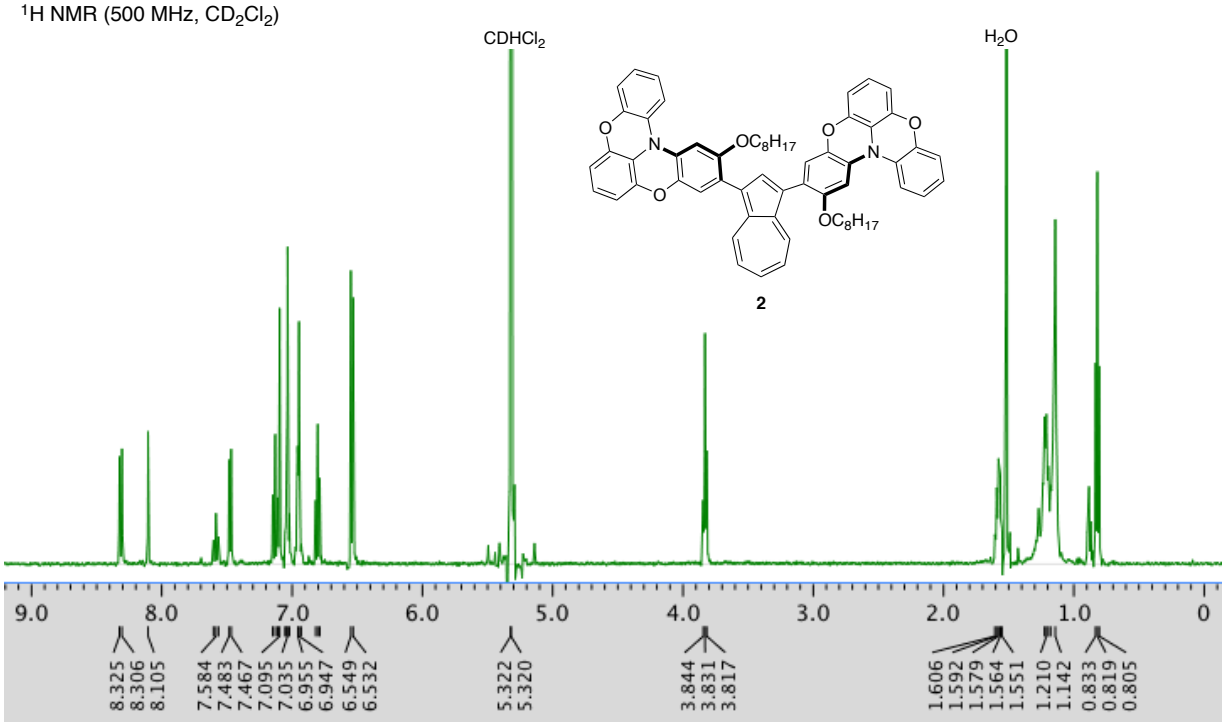

^{13}C NMR (125 MHz, CD_2Cl_2)

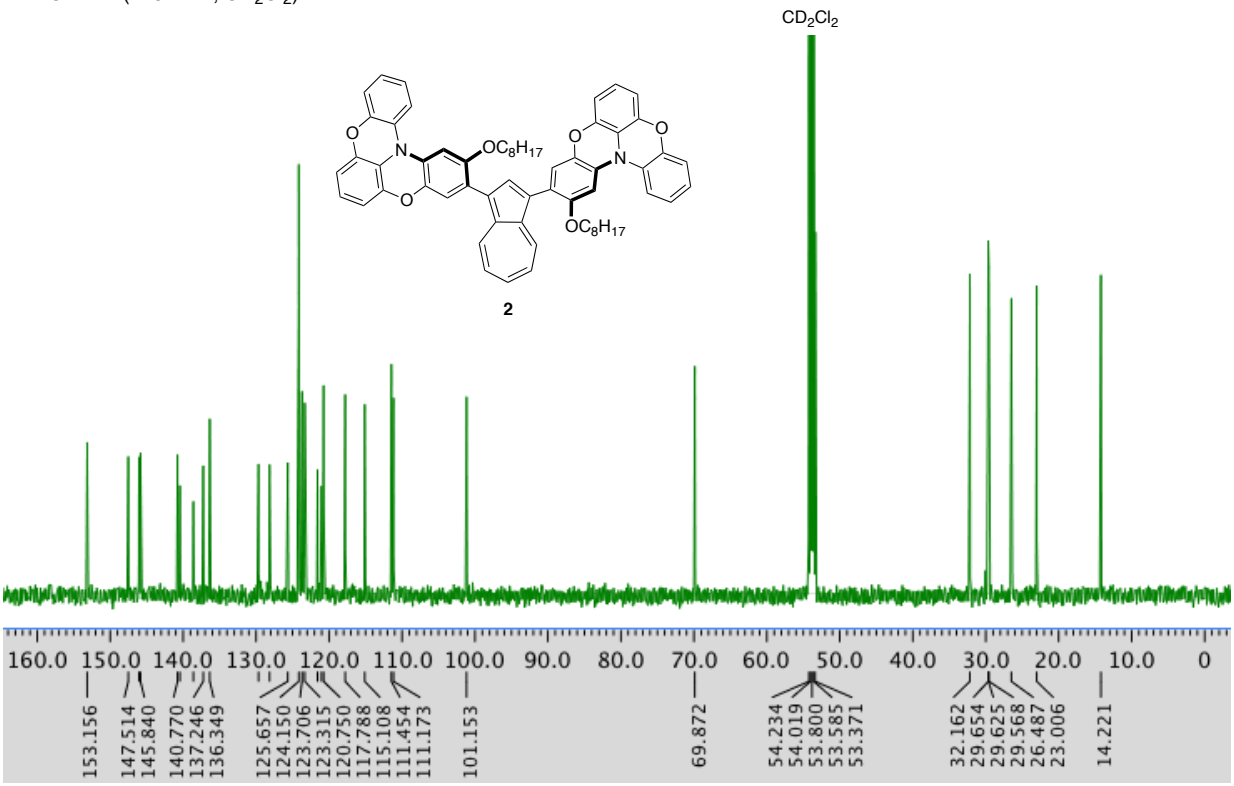

^{1}H NMR (500 MHz, CD_2Cl_2)

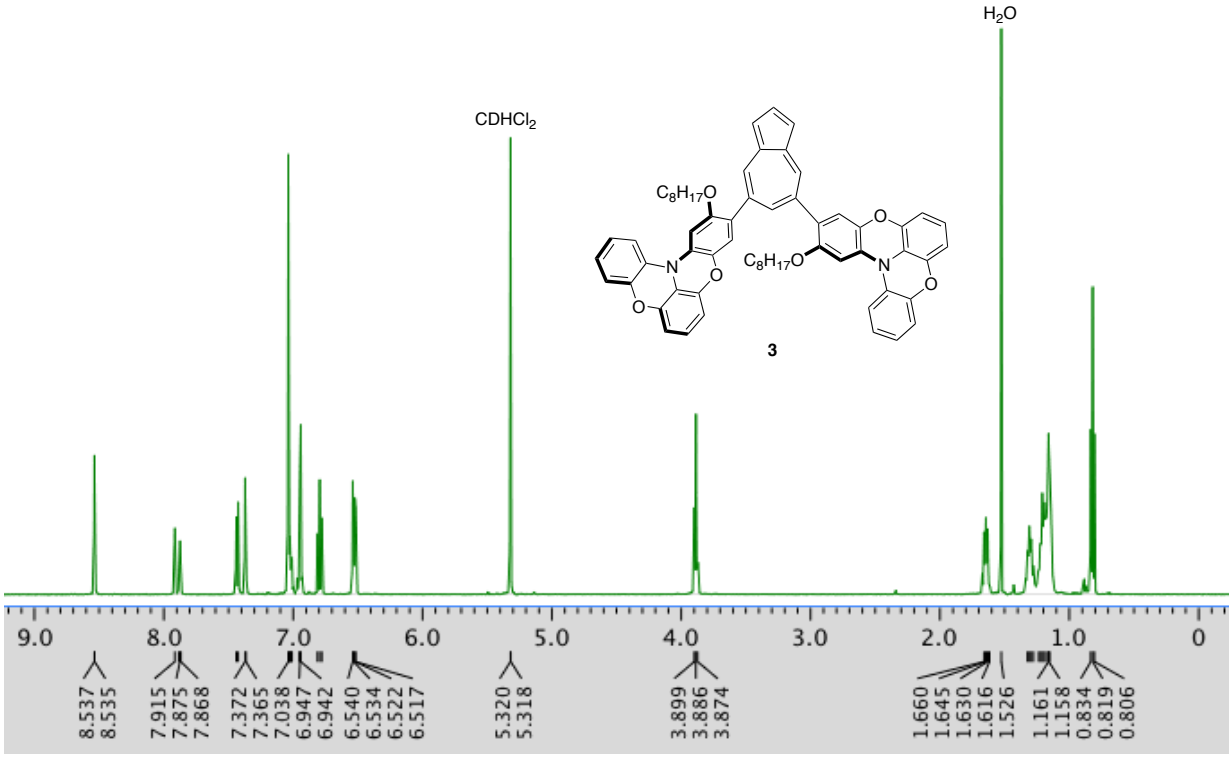

^{13}C NMR (125 MHz, CD_2Cl_2)

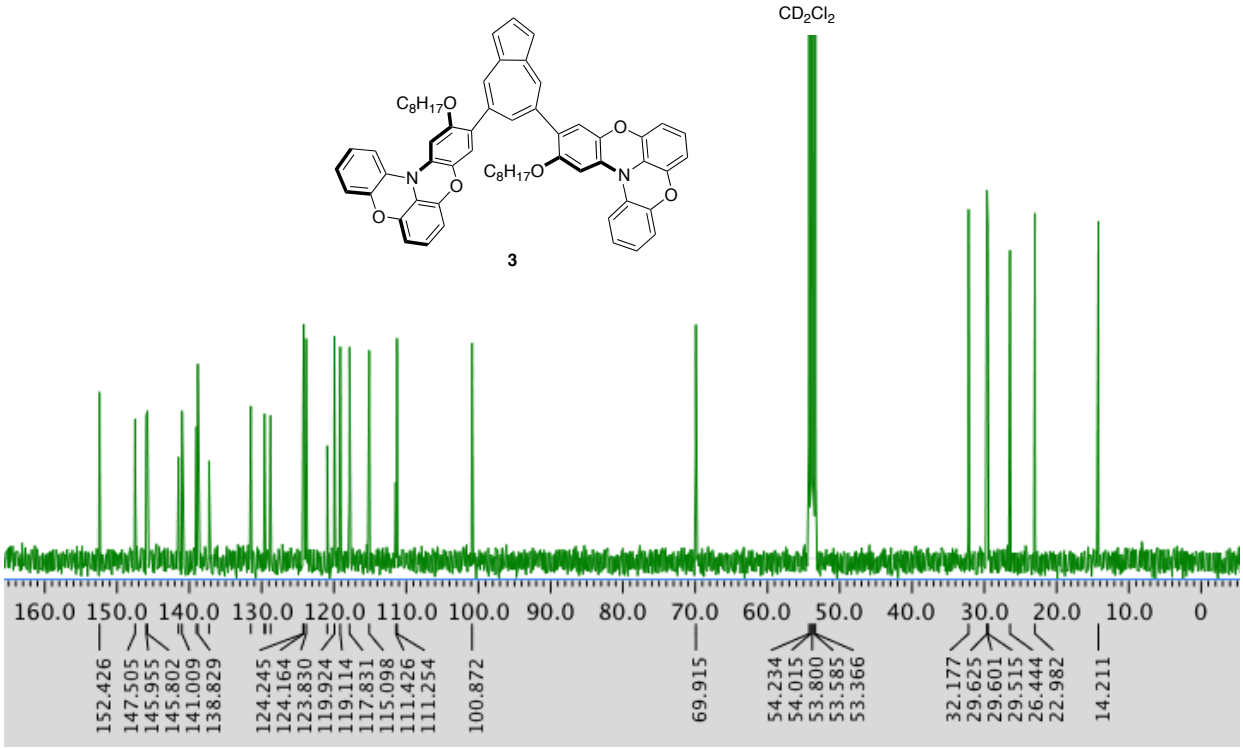

^{1}H NMR (500 MHz, CD_2Cl_2)

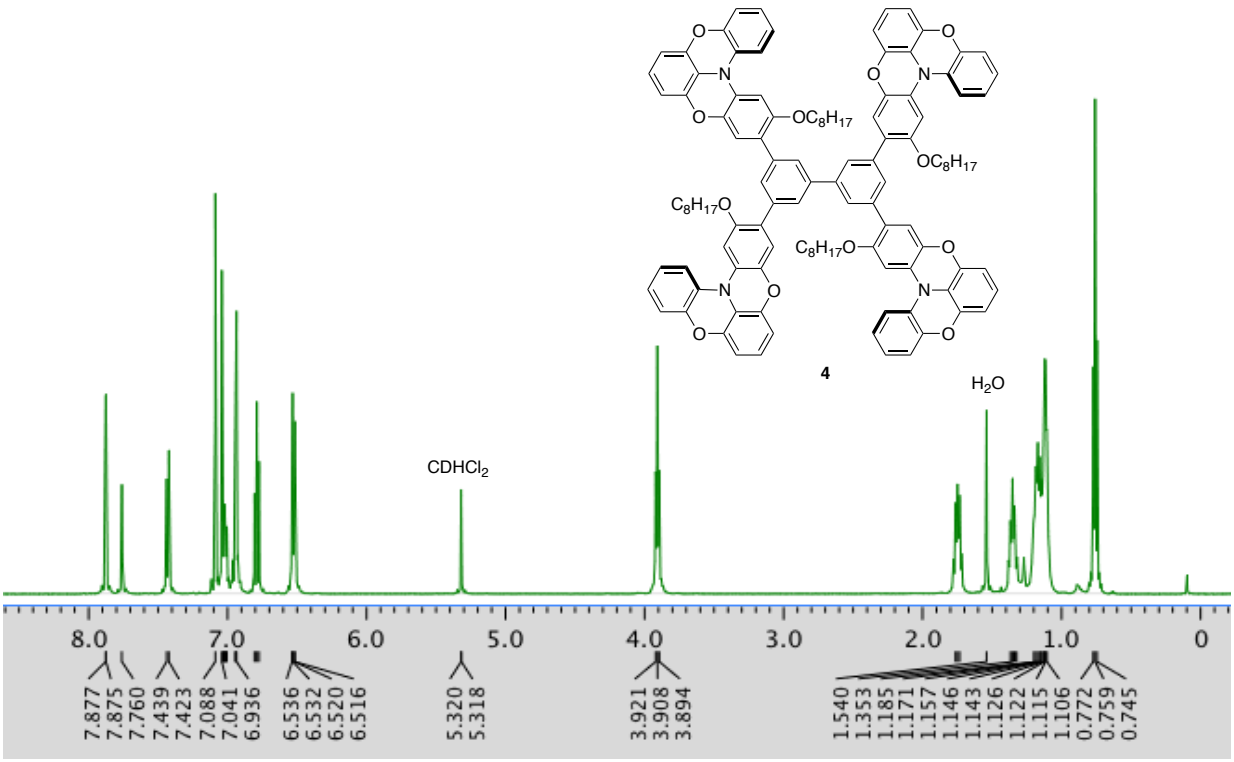

^{13}C NMR (125 MHz, CD_2Cl_2)